Designs of Substrate Integrated Waveguide (SIW) and Its Transition to Rectangular Waveguide

by

Ya Guo

A thesis submitted to the Graduate Faculty of
Auburn University
in partial fulfillment of the
requirements for the Degree of
Master of Science

Auburn, Alabama
May 10, 2015

Keywords: Substrate Integrated Waveguide (SIW), Rectangular Waveguide (RWG), Waveguide transition, high frequency simulation software (HFSS), genetic algorithm (GA)

Approved by

Michael C. Hamilton, Chair, Assistant Professor of Electrical & Computer Engineering
Bogdan M. Wilamowski, Professor of Electrical & Computer Engineering
Michael E. Baginski, Associate Professor of Electrical & Computer Engineering

Abstract

There has been an ever increasing interest in the study of substrate integrated waveguide (SIW) since 1998. Due to its low loss, planar nature, high integration capability and high compactness, SIW has been widely used to develop the components and circuits operating in the microwave and millimeter-wave region. For the integrated design of SIW and other transmission lines, the design of feasible and effective transitions between them is the key.

In this work, substrate integrated waveguides for E-band, V-band and Q-band are designed and accurately modeled, their high frequency performances are simulated and analyzed with the Ansys' High Frequency Structure Simulator (HFSS). Additionally, two kinds of transitions between RWG and SIW are explored for narrow band 76-77 GHz and broad bands 77-81 GHz, 56-68 GHz and 40-50 GHz, and they are simulated in HFSS. The loss of the transition portion is extracted by linear fitting method. Genetic algorithm is also used to find the optimal dimensions and placements of the transitions for broad operative bands. All in all, the purpose of this thesis is to design proper SIW and proper RWG-to-SIW transitions with minimum loss, and the scattering parameters are mainly used to analyze their high frequency performance.

Acknowledgments

I sincerely thank Dr. Michael C. Hamilton, my academic advisor, for giving me the valuable opportunity to work in his research group; throughout my time within his research group, he provides every bit of guidance and advice as he can in helping me step into the professionalism of mm-wave transmission line design. Also I gratefully acknowledge the guidance, discussion and contributions from Dr. Jeorge S. Hurtarte and Mr. Ken Degan, both of Teradyne, Inc., during a project associated with much of the work presented in the Thesis. I also sincerely thank Teradyne, Inc. for financial support during the associated project.

Table of Contents

List of Tables

List of Figures

List of Abbreviations

SIW	Substrate Integrated Waveguide
PCB	Printed Circuit Board
LTCC	Low-temperature Co-fired Ceramic
RWG	Rectangular Waveguide
CPW	Coplanar Waveguide
GCPW	Grounded Coplanar Waveguide
HFSS	High Frequency Structural Simulator
S-Parameter	Scattering Parameters
mm-Wave	Millimeter-Wave
WR	Waveguide Rectangular
GA	Genetic Algorithm
HSIW	Hollow Substrate Integrated Waveguide

Chapter 1

Introduction

Substrate Integrated Waveguide (is also named as “Laminated Waveguide” or “Post-wall Waveguide”) was firstly proposed in 1998 for microwave and millimeter-wave applications. In the following decade, relevant studies continued rapidly mainly focusing on the accurate modeling, wave propagation mechanisms, dispersion characteristics, and design and fabrication considerations of SIW. Meanwhile, a variety of substrate-integrated waveguide components, circuits and antennas have been developed and implemented, such as SIW passive circuits (e.g. filters and couplers), SIW active circuits (e.g. oscillators, mixers and amplifiers) and SIW antennas [1-5]. All of these studies and work demonstrate that this interesting planar waveguide —SIW is promising for use in mm-wave technologies and areas, including wireless networks, radars, biomedical devices, and etc.

As a planar form of waveguide, SIW can be a promising candidate for the traditional non-planar rectangular waveguide, compatible with existing planar processing techniques such as standard printed circuit board (PCB) or low-temperature co-fired ceramic (LTCC). Compared to the classic rectangular waveguide, SIW preserves some similar characteristics to RWG, and exhibits its unique advantages than SIW as well, such as [5]:

- similar propagation characteristics including the field pattern and dispersion characteristics to conventional RWG;
- high quality-factor, high power-handling capability, self-consistent electrical shielding;

- high integration capability with other planar components such as CPW, microstrip on the same substrate.

1.1 Transitions between SIW and other transmission lines

Various kinds of transmission lines such as coplanar waveguide, microstrip, rectangular waveguide and SIW play important roles in microwave and millimeter wave circuit design, while there are many commercial products designed based on their different format. Therefore, to make integration of these different circuits, the hybrid design of these transmission lines are necessary.

Particularly, microstrip-to-SIW transitions are typically designed in planar platform, while the microstrip and SIW are integrated on the same substrate and interconnected via a simple taper [5, 6]. The configuration is shown in Figure 1.1 [5]:

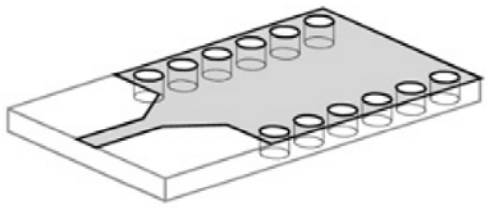

Figure 1.1 Microstrip-to-SIW transition based on a taper [5].

For the design of coplanar-to-SIW transitions, one proposed scheme exploits a current probe to transfer power between the two planar transmission lines. As shown in Figure 1.2, the current flowing in the GCPW can create a magnetic field when it goes through the coupling probe, which matches the magnetic field inside the SIW, and then the coupling between the GCPW and SIW is achieved [7]. Another transition structure was proposed in [8], the CPW and SIW are also integrated on the same substrate, and the coplanar waveguide has a 90˚ bend on each slot inside the SIW structure, as shown in Figure 1.3 [5].

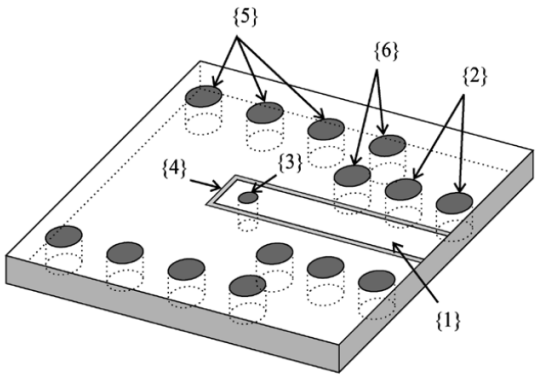

Figure 1.2 GCPW-to-SIW transition based on a current probe [7].

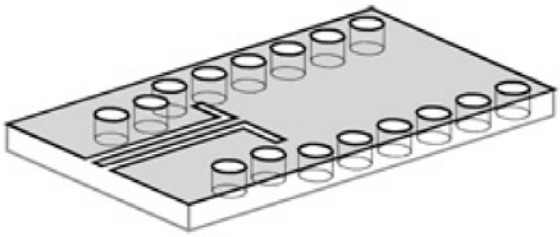

Figure 1.3 CPW-to-SIW transition based on a 90˚ bend [5].

Additionally, some solutions for RWG-to-SIW transitions have been proposed. One kind of transition proposed in [9] is based on a radial probe extended from the SIW and inserted into the tapered metallic waveguide. Another kind of step transformers connecting the RWG and SIW in parallel is proposed in [10], these transformers are rectangular waveguides with different dimensions, seen from the RWG side to SIW side, the dimensions of the transformers decreases successively to match the impedance between RWG and SIW gradually. Besides transferring energy between SIW and RWG in parallel, there are some other transitions applied to couple the energy between SIW and RWG vertically in geometry. By etching one slot or two slots on the metallic layer of SIW as the transitions, surface-mount the RWG to SIW and couple the energy through the slot opening(s) are effective solutions for narrow operative band [11, 12]. While for broad operative band, transitions between RWG and SIW are proposed in [13] and [14]. Similarly an aperture is cut on the metallic layer of SIW, the incident wave is transmitted from

RWG into SIW through this aperture, but differently, the vias-wall width around the aperture is made larger than the core SIW line width (defined by the center-to-center distance between the two rows of vias) and presents a gradually step shape. The broadened vias-wall is designed with rhombus-like shape in [13] while designed with rectangular-like shaped in [14]. The design strategies of these vertically located RWG-to-SIW transitions are discussed in Chapter 3 in detail.

1.2 Outline of This Thesis

The first topic of this thesis, presented in Chapter 2, is the study of SIW design method and properties. We show the accurate modeling and design strategy of SIW, from the calculation or selection of each dimension, to minimizing the leakage or dispersion loss of SIW from different aspects. Based on the design rules and strategy, we design different-dimension SIWs for different operative bands, and they show good high frequency performances, which validate that the SIW design method is reliable and reproducible. Moreover, we show the advantages and disadvantages of SIW by comparing it with other transmission lines, while the RWG, Stripline, Microstrip, and GCPW counterparts of SIW are simulated and analyzed as well.

The second topic of this thesis, presented in Chapter 3 is the study of transition between standard rectangular waveguide and SIW for either narrow band or broad band. Opening a narrow slot or broad aperture on the metallic layer of SIW is a simple and feasible way to couple the energy between RWG and SIW [11, 14]. The design strategies of these transitions are discussed, and different-dimension transitions for different operative bands are designed and simulated to validate the design method. Additionally, a linear fitting method is proposed to exact the loss of the sole transition part. Finally we implement genetic algorithm to look for the optimal dimensions and placements of the transitions for broad bands.

This thesis concludes with Chapter 4, where the work of this thesis is summarized and the major conclusions are derived. Possible future work and prospects are also discussed briefly in this concluding chapter.

Chapter 2

Design and Comparison of Substrate Integrated Waveguide and Other Transmission Lines

2.1 SIW Structure Design

SIW (substrate integrated waveguide) are integrated waveguide-like and planar structures, which can be created by adding metallic ground planes to the top and bottom of a dielectric substrate, two periodic rows of metallic vias or slots are used to connect the top and bottom ground planes [15, 16], as shown in Figure 2.1.

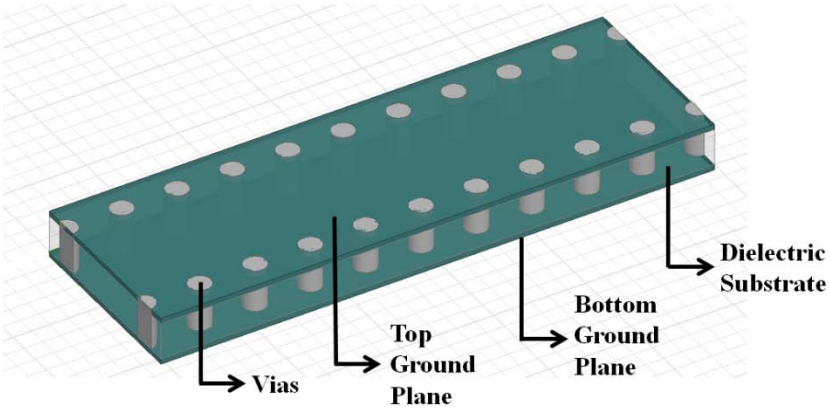

Figure 2.1 Substrate Integrated Waveguide.

2.1.1 SIW Modeling and Design Strategy

The design technique of SIW is mapped from the rectangular waveguide design strategy; a substrate integrated waveguide can be equivalent to its dielectric filled metallic rectangular waveguide [17, 18]. The parameters shown in Figure 2.2 play important roles in the SIW design. In Figure 2.2, 'd' is diameter of vias, 'p' is the period between the vias, 'a' is center to center

distance between both rows of vias, and 'h' is the height of the dielectric substrate. If the geometry of SIW is designed properly, the energy leaking between consecutive vias is negligible.

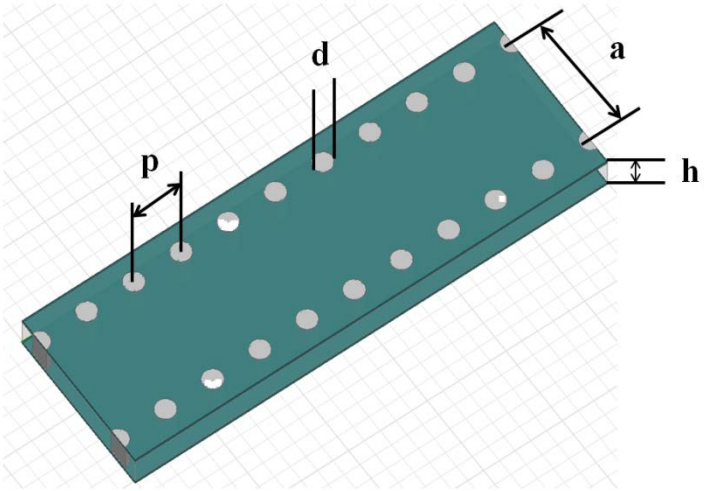

Figure 2.2 Geometry of SIW.

Consider a SIW as its equivalent dielectric filled rectangular waveguide with an effective width [17], and both of them have the same cutoff frequency. As shown in Figure 2.3, 'a_{equ}'is the width of equivalent dielectric filled waveguide counterpart to a SIW.

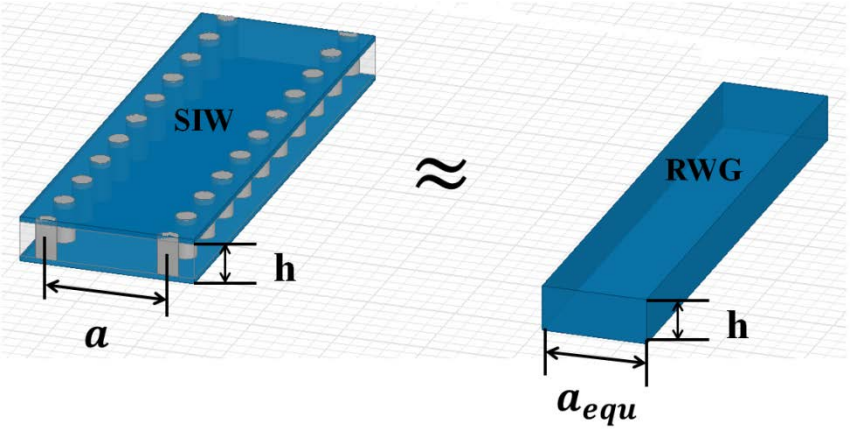

Figure 2.3 SIW and its equivalent RWG.

Known the velocity of light 'c' and the dielectric constant 'ε_r', the cutoff frequency 'f_c' can be defined as below [16]:

$$f_c = \frac{c}{2a_{equ}\sqrt{\varepsilon_r}} \quad (2.1)$$

Here the cutoff frequency 'f_c' are chosen as same as the recommended cutoff frequency of operation of standard rectangular waveguide for different bands. Therefore we can get another form of equation (2.1) and calculate 'a_{equ}':

$$a_{equ} = \frac{c}{2f_c\sqrt{\varepsilon_r}} \quad (2.2)$$

The proper selections of via diameter 'd' and the periodic distance 'p' between vias can minimize the leakage loss of SIW. In order to guarantee the SIW structure physically realizable, the vias diameter should be less than the periodic distance [16]:

$$d < p \quad (2.3)$$

Since SIW is a periodic guided wave structure, any electromagnetic bandstop effects over the waveguide operating bandwidth should be avoided. Furthermore, considering the actual manufacturing limitation, that is the production time, complexity and feasibility of SIW are proportional to the numbers of vias; generally the number of vias should not exceed 20 percent of wavelength [16]. Therefore use the given condition shown below:

$$0.05 < \frac{p}{\lambda_c} < 0.25 \quad (2.4)$$

Then the center to center distance 'a' between both rows of vias can be determined as below [16]:

$$a = a_{equ} + \frac{d^2}{0.95p} \quad (2.5)$$

This thesis develops the SIW structures for the following four mmWave frequency bands: 77-81 GHz, 76-77 GHz, 56-68 GHz and 40-50 GHz. Since the waveguide E band is the range of radio frequencies from 60 GHz to 90 GHz (covering 77-81 GHz and 76-77 GHz), the waveguide V band has a frequency band of operation from 50 GHz to 75 GHz (covering 56-68 GHz), and

the waveguide Q band ranges from 33 GHz to 50 GHz (covering 40-50 GHz), three different SIW structures working in these three different operation bands – E band, V band and Q band are designed, respectively.

As mentioned before, the selections of via diameter 'd' and the periodic distance 'p' between vias have big effects on the leakage loss of SIW, while the center to center distance 'a' between both rows of vias has a great impact on the cutoff frequency of lowest order mode for SIW working in different bands. In ANSYS HFSS software, set up a model for SIW working in E-band. The length of SIW is 1 inch, the dielectric substrate material is Megtron 6 with dielectric constant ('ε_r') 3.34 and loss tangent ('$tan\delta$') 0.002, and via diameter via diameter 'd' and the periodic distance 'p' between vias are calculated as 7 mil and 14 mil, respectively, and the material of top and bottom metallic ground planes are chosen as copper with conductivity ('σ') 5×10^7 S/m. The HFSS simulation model is shown in Figure 2.4:

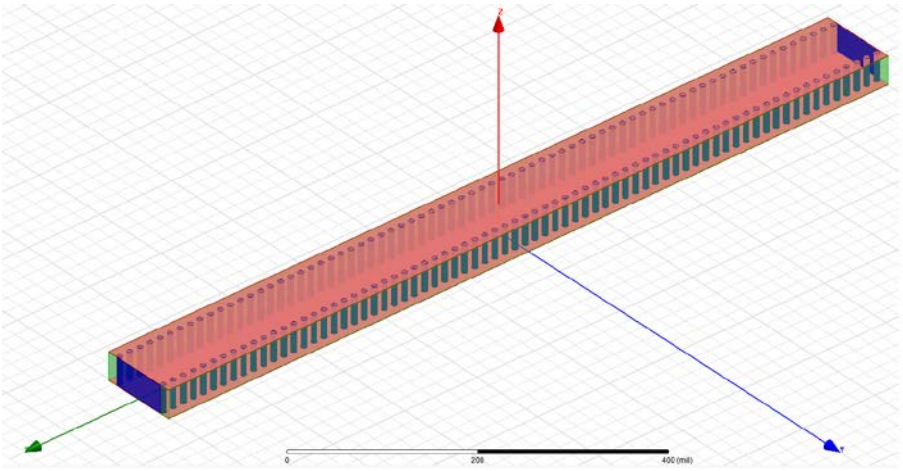

Figure 2.4 HFSS simulation model of 1 inch long E band SIW.

Change the value of 'a' (the center to center distance between both rows of vias) from 25mil to 45mil, the reflection and transmission coefficients of the E band SIW are shown in Figure 2.5 and Figure 2.6, respectively.

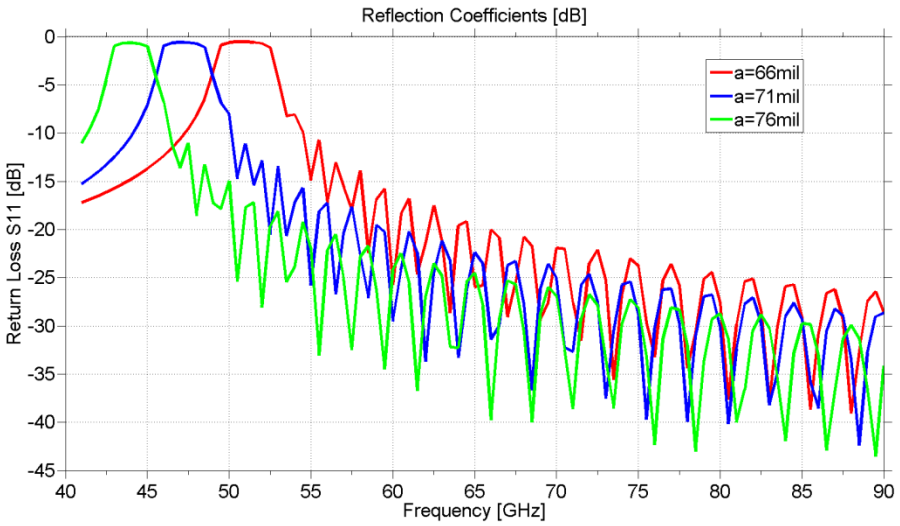

Figure 2.5 Reflection coefficients of 1 inch long E band SIW with different ‘a’.

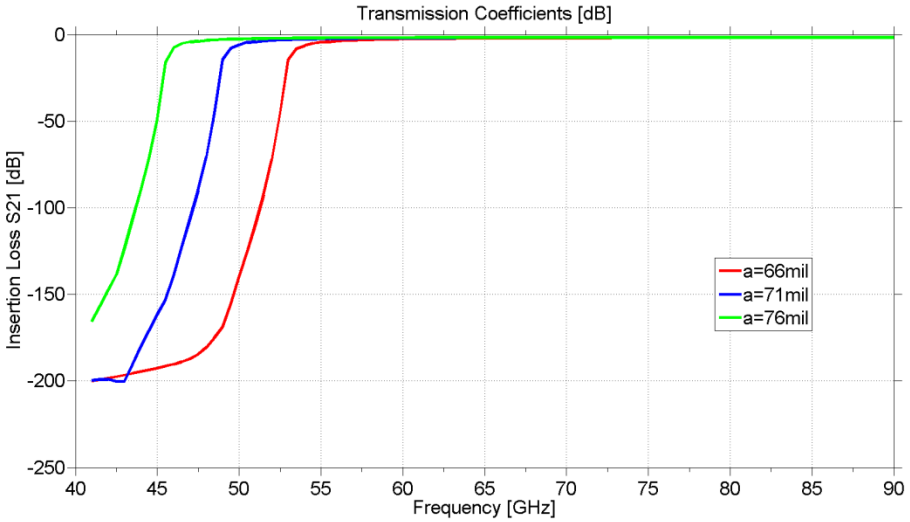

Figure 2.6 Transmission coefficients of 1 inch long E band SIW with different ‘a’.

From the high frequency performance of the E band SIW with different ’a’, we can see that the center to center distance between both rows of vias affects the cutoff frequency for SIW. The bigger ’a’ is, the smaller cutoff frequency SIW has. Since the calculation of ’a’ from the equations mentioned above is not accurate enough to achieve the exact cutoff frequency that

SIW should has, according to the relations between 'a' and cutoff frequency, we can optimize 'a' to get SIW achieve its desired cutoff frequency.

However, unlike the other kinds of transmission lines such as microstrip or stripline, the substrate thickness 'h' has negligible effect on the high frequency performance of SIW. Also take a 1 inch long E band SIW as the simulation model, the center to center distance 'a' between both rows of vias is 71mil, the other dimensions are all kept the same except the substrate thickness 'h'. Change the range of 'h' from 25mil to 45mil, the reflection coefficients and transmission coefficients of the E band SIW are shown in Figure 2.7 and Figure 2.8, respectively.

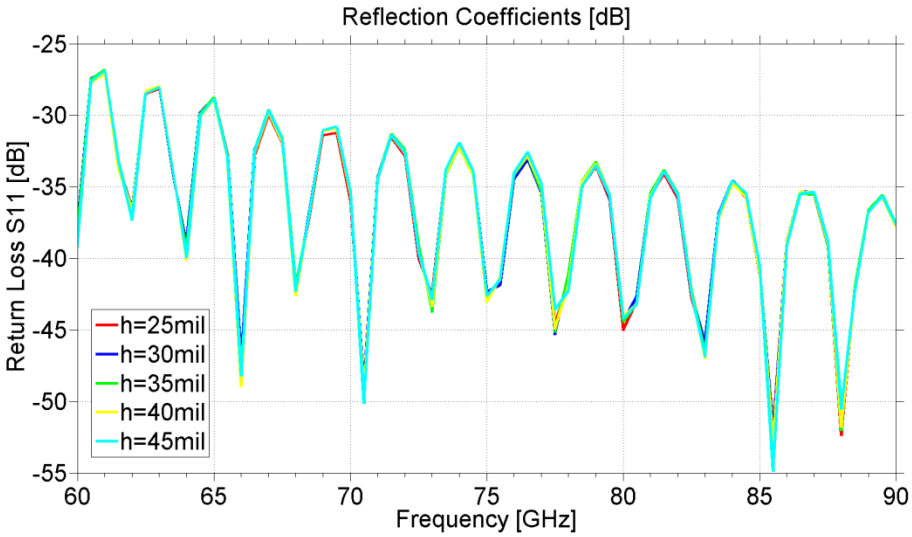

Figure 2.7 Reflection coefficients of 1 inch long E band SIW with different 'h'.

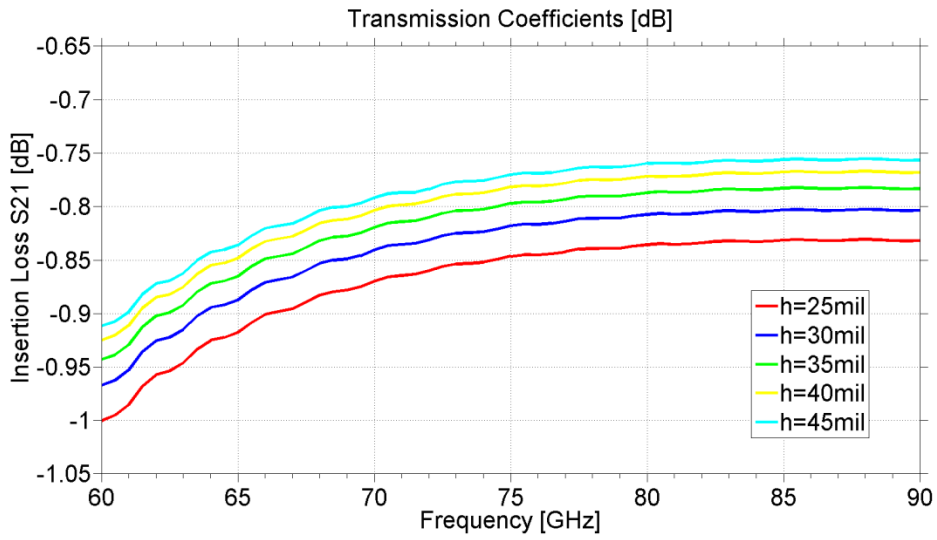

Figure 2.8 Transmission coefficients of 1 inch long E band SIW with different 'h'.

2.1.2 Loss Minimization for SIW

Proper design of SIW dimension can minimize the energy leaking between consecutive vias and get the exact cutoff frequency for waveguide band, also the properties of substrate material and metallic ground plane material have significant effects on the energy loss of SIW, that is the dielectric material's and metallic material's inherent dissipation of electromagnetic energy into, e.g., heat cannot be ignorable. The dielectric loss can be parameterized in terms of loss tangent ('$tan\delta$'), and the metallic loss can be parameterized in terms of electrical conductivity ('σ').

Use the previous 1 inch E band SIW model mentioned above, 'd' is 7 mil, 'p' is 14 mil, 'a' is 71 mil, and 'h' is 35 mil; The ground planes use 0.5 oz. copper with conductivity ('σ') 5×10^7 S/m, the thickness of the copper ground plane is 17.5 um. The dielectric substrate material is Megtron 6 with dielectric constant ('ε_r') 3.34, however its loss tangent ('$tan\delta$') ranges from 0 to 0.005. The reflection and transmission coefficients (return loss and insertion loss) of SIW for different dielectric loss tangents are shown in Figure 2.9 and Figure 2.10, respectively.

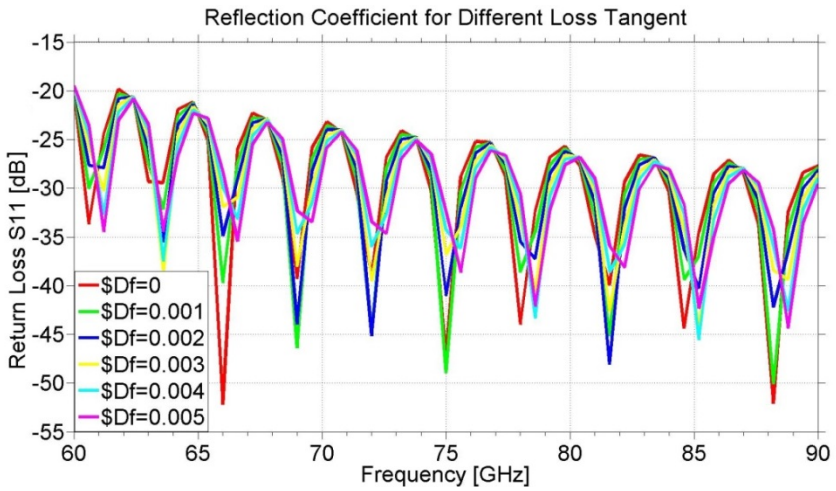

Figure 2.9 Reflection coefficient of 1 inch long E band SIW for different loss tangents.

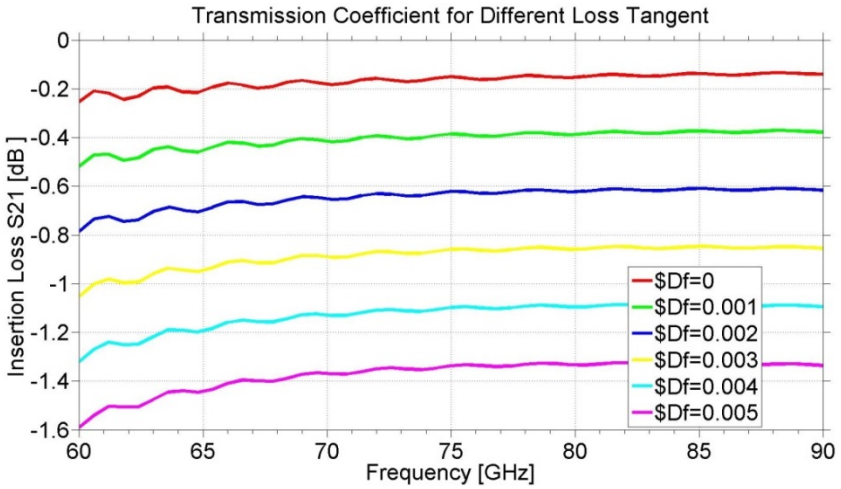

Figure 2.10 Transmission coefficient of 1 inch long E band SIW for different loss tangents.

Take the same 1 inch E band SIW as the simulation model, but the loss tangent of the substrate material is set as 0 (which means the dielectric loss of SIW is 0), then change the metallic material of the ground planes into perfect conductor instead of copper, the electrical conductivity (‘σ’) of perfect conductor is 1×10^{30} S/m. The reflection and transmission coefficients (return loss and insertion loss) of SIW for perfect conductor as ground planes are shown in Figure 2.11 and Figure 2.12, respectively.

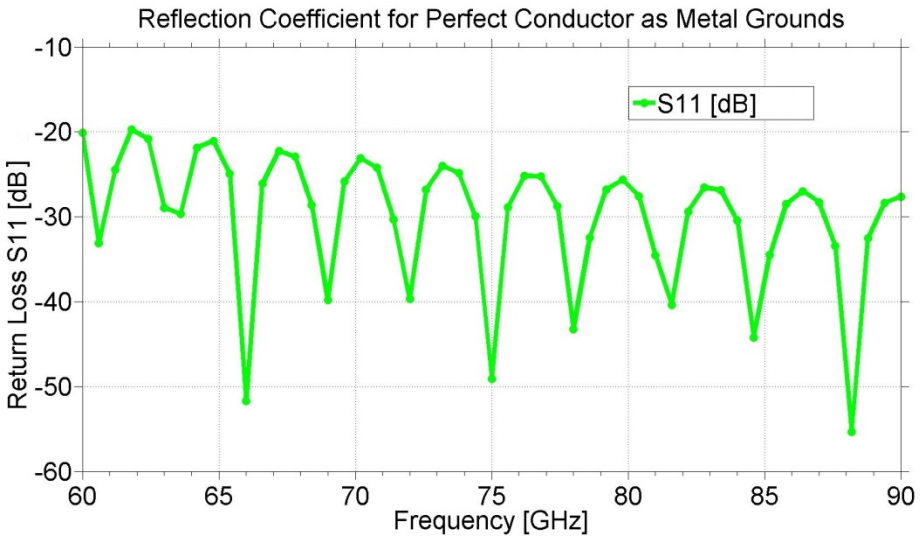

Figure 2.11 Reflection coefficient of 1 inch E band SIW for perfect conductor as ground planes.

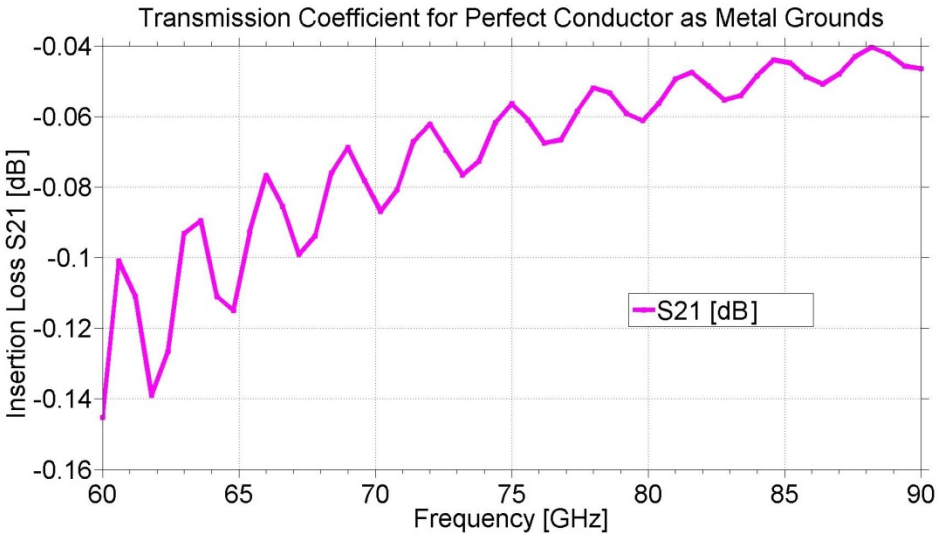

Figure 2.12 Transmission coefficient of 1 inch E band SIW for perfect conductor as ground planes.

All of these results support the idea that, in order to minimize the loss of SIW, besides the proper designs of 'd' (via diameter), 'p' (the periodic distance between vias) and 'a' (the center to center distance between both rows of vias), choosing proper dielectric material with low loss tangent for substrate and smooth metallic material with high electrical conductivity for ground

planes can also effectively reduce the loss of SIW. However, the effect of the substrate height for the SIW high frequency performance can be negligible.

2.1.3 SIW Design Results and High Frequency Performance for Different Bands

According to the design strategy explained in section 2.1.1, and considering the actual fabrication tolerance (while the actual manufacturing accuracy is 0.5mil), finally the Megtron 6 with dielectric constant ('ε_r') 3.34 and loss tangent ('$tan\delta$') 0.002 is selected as the substrate material, and 0.5 oz. copper with conductivity ('σ') 5×10^7 S/m is selected as the metallic ground material. The detailed dimensions of SIW for three different operation bands – E band, V band and Q band are shown in Table 2.1 as below:

	d	p	a	h
E band (60 GHz ~ 90 GHz)	7 mil	14 mil	71 mil	35 mil
V band (50 GHz ~ 75 GHz)	8.5 mil	17 mil	86 mil	35 mil
Q band (33 GHz ~ 50 GHz)	13 mil	26 mil	130.5mil	35 mil

Table 2.1 Parameters for SIW design for different bands.

The simulation results for S parameters (S11, S21, S22 and S12) of E band SIW and its E-Field are shown below in Figure 2.13 and Figure 2.14, respectively.

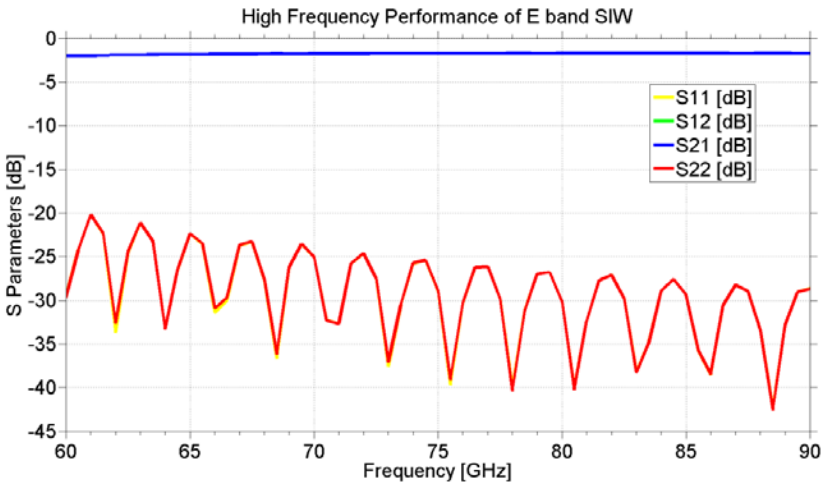

Figure 2.13 E band SIW S-Parameters.

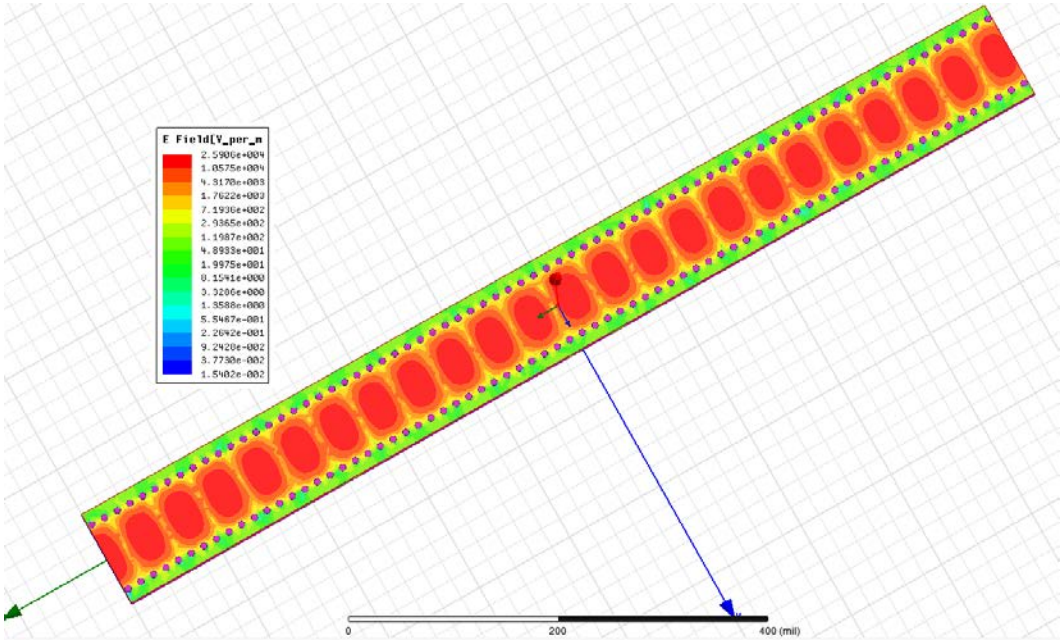

Figure 2.14 E band SIW E-field plot at 90 GHz.

The simulation results for S parameters (S11, S21, S22 and S12) of V band SIW and its E-Field are shown below in Figure 2.15 and Figure 2.16, respectively.

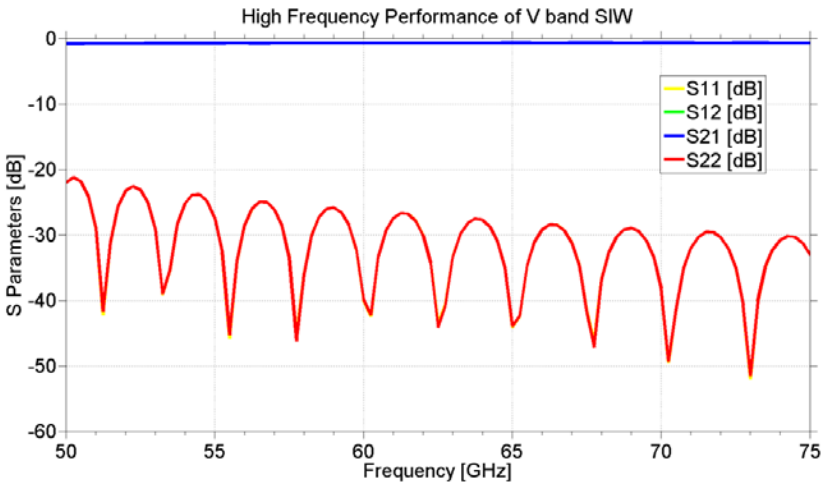

Figure 2.15 V band SIW S-Parameters.

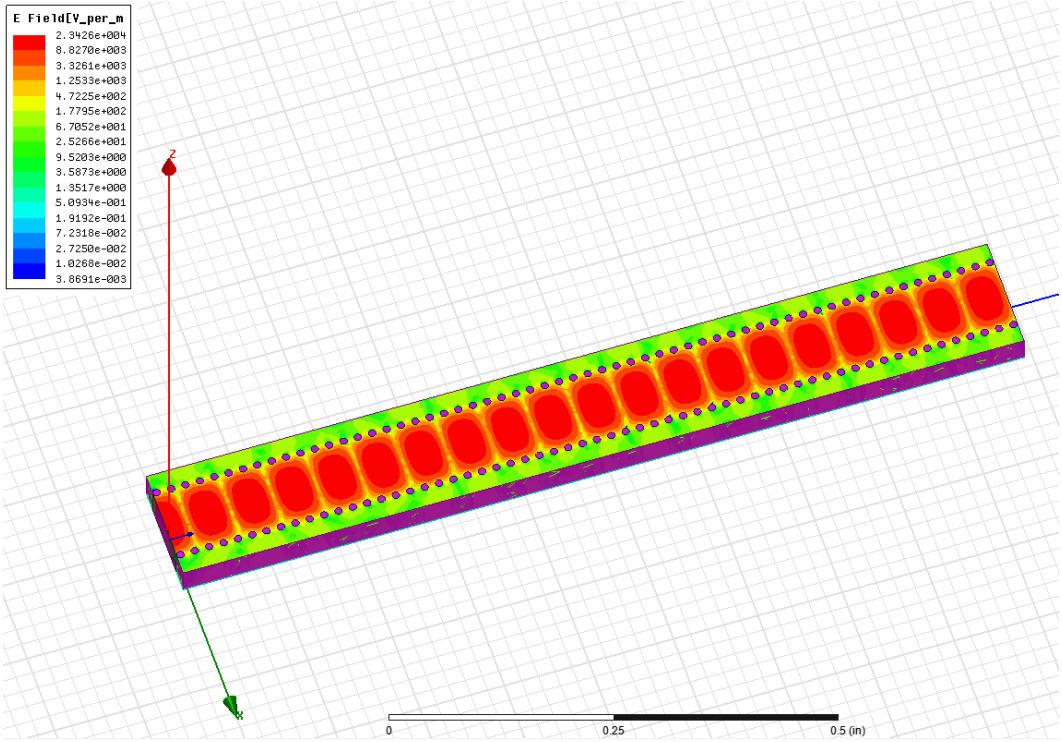

Figure 2.16 V band SIW E-field plot at 75 GHz.

The simulation results for S parameters (S11, S21, S22 and S12) of Q band SIW and its E-Field are shown below in Figure 2.17 and Figure 2.18, respectively.

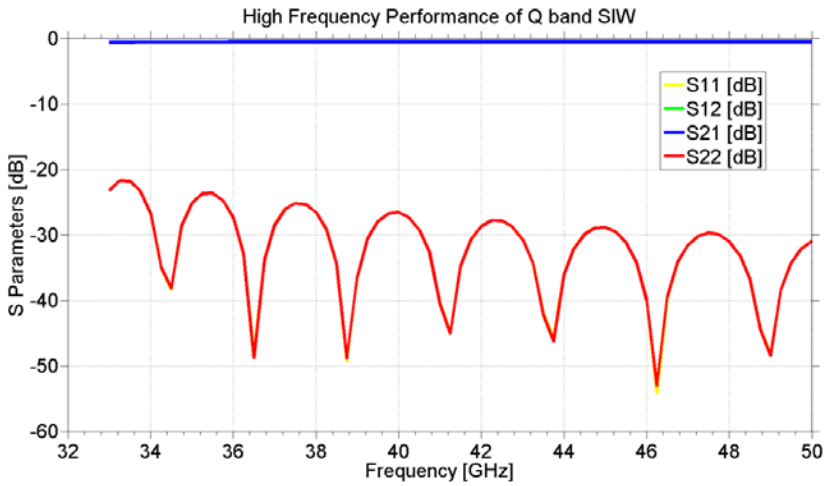

Figure 2.17 Q band SIW S-Parameters.

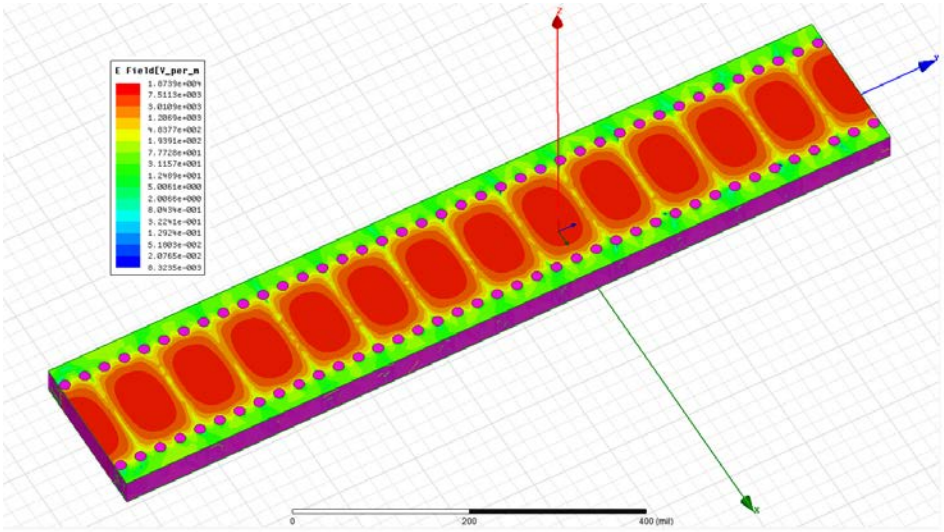

Figure 2.18 Q band SIW E-field plot at 50 GHz.

For E band SIW, the return loss is below -20 dB and the insertion loss is above -2 dB in the whole waveguide band. For V band SIW, the return loss is below -21 dB and the insertion loss is above -0.9 dB in the whole waveguide band. For Q band SIW, the return loss is below -20 dB and the insertion loss is above -0.6 dB in the whole waveguide band. They all achieve good high

frequency performance. As shown in the E-field plots for different bands, as the electromagnetic wave propagates along the body of SIW, there will be some inevitable wave energy attenuation.

2.2 Design of Other Transmission Lines

In order to find out the advantages and disadvantages of SIW over the other transmission lines and make comparison, standard rectangular waveguide, microstrip line, stripline, and CPW are also designed and simulated for different bands – E band, V band and Q band.

2.2.1 Standard RWG

The Electronic Industries Alliance (EIA) has developed a set of waveguide design standards for practice. According to the standards, WR (Waveguide Rectangular) 12 is stipulated for E band, and the inner dimensions of its opening is 0.122×0.061 inch; WR 15 is stipulated for V band, and the inner dimensions of its opening is 0.148×0.074 inch; and WR 22 is stipulated for Q band, and the inner dimensions of its opening is 0.224×0.112 inch. The wall thickness of these standard rectangular waveguides (RWG) is 0.04 inch [19].

The HFSS simulation models of 1 inch long standard RWG for E band, V band and Q band are shown in Figure 2.19.

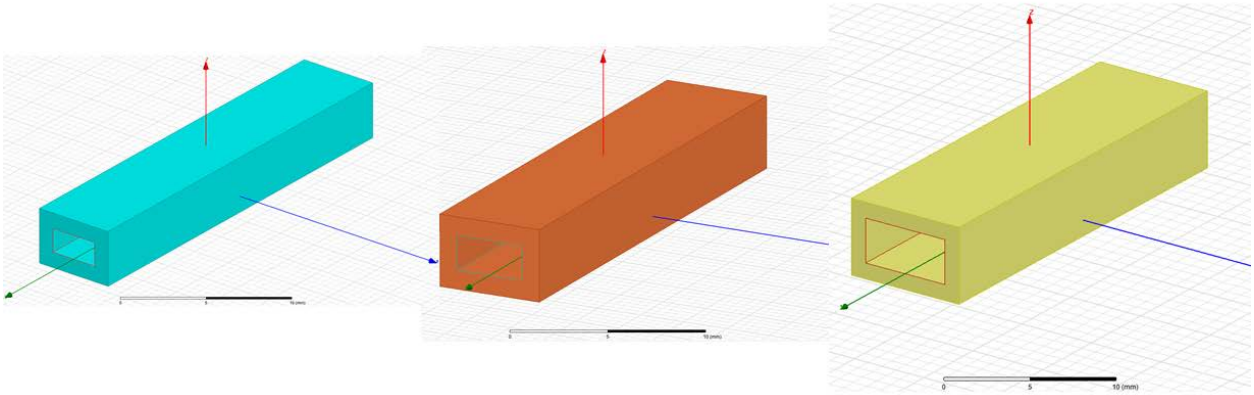

Figure 2.19 HFSS simulation models of 1 inch long standard RWG, they are WR 12, WR 15 and WR 22 from the left to the right.

The high frequency performance for WR 12, WR 15 and WR 22 are shown in Figure 2.20, Figure 2.21, Figure 2.22, respectively.

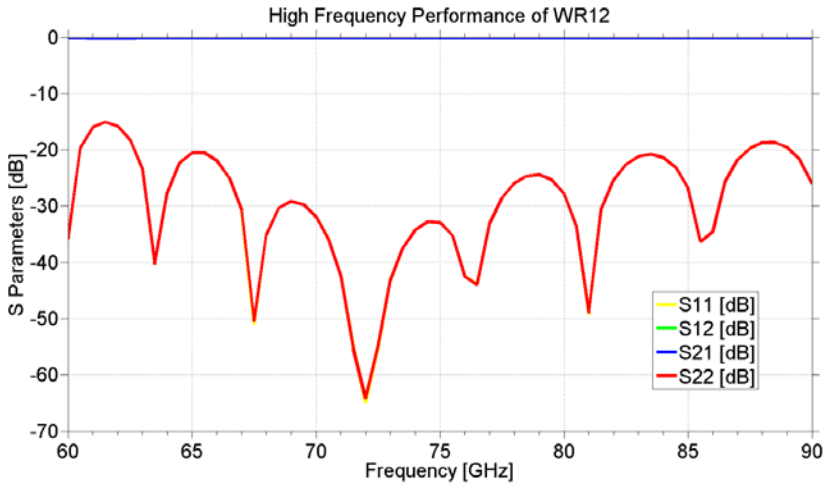

Figure 2.20 WR 12 S-Parameters.

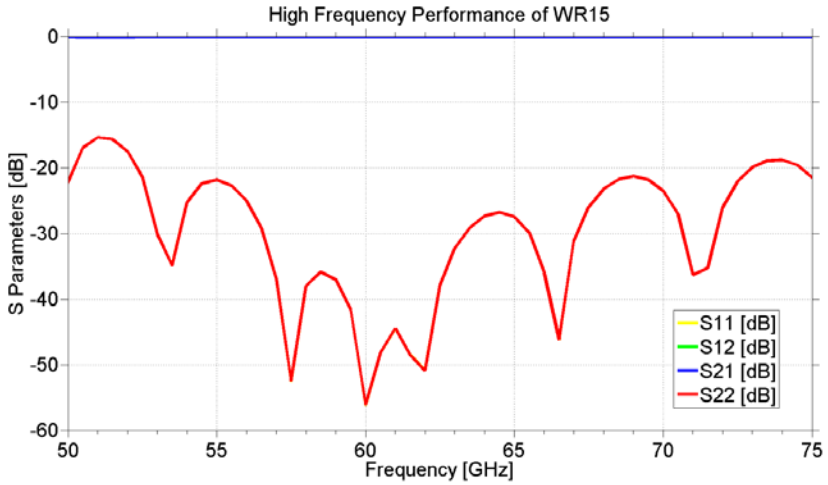

Figure 2.21 WR 15 S-Parameters.

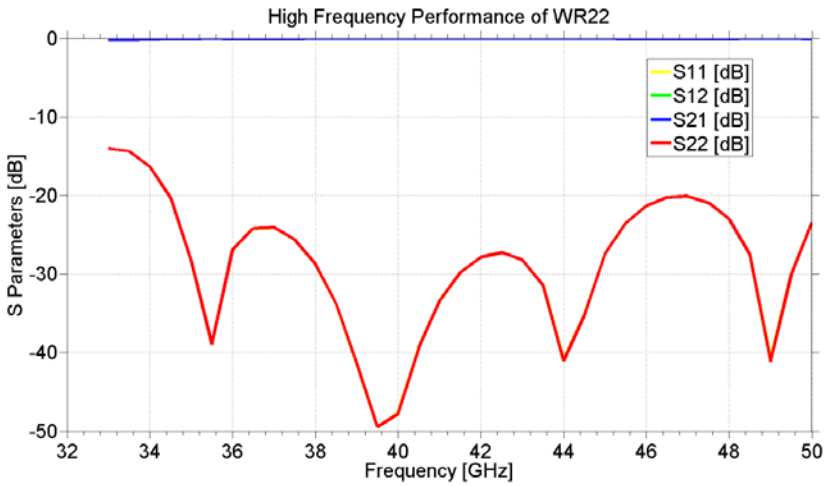

Figure 2.22 WR 22 S-Parameters.

From the simulation results, we can see that the standard rectangular waveguides have good high frequency performance. The return loss of WR 12, WR 15 and WR 22 is all below -14 dB and the insertion loss is all above -0.3 dB in their respective waveguide bands. Since the RWG are air-filled, we can approximately think that no dielectric loss caused during the wave propagation in RWG. However, we can also observe that the dimensions of RWG are much larger than their SIW counterparts, so they are much bulkier than SIW.

2.2.2 Stripline Design

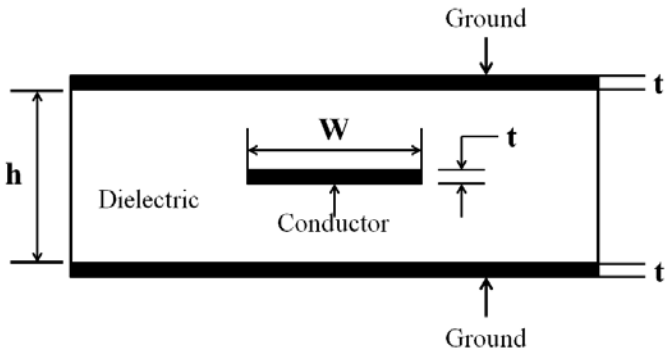

Figure 2.23 Stripline cross-section.

Design 1 inch long 50Ω (characteristic impedance) Stripline for the three different operation bands (76-81 GHz, 40-50 GHz, and 56-68 GHz). Select Megtron 6 with dielectric constant ('ε_r') 3.34 and loss tangent ('$tan\delta$') 0.002 as the dielectric material, and use 0.5 oz. copper with conductivity ('σ') 5×10^7 S/m as the internal conductor and ground material, while the thickness "t" of conductor and ground plane is 17.5 um.

The characteristic impedance of the TE_{10} mode for Stripline does not vary with frequency, since Stripline contains only a single conductor in the region confined by the two metallic ground planes [20]. The Stripline characteristic impedance can be approximated using the simple equation [20]:

$$Z_0 = \frac{30\pi}{\sqrt{\varepsilon_r}} \frac{h}{W_e + 0.441h} \ (\Omega) \tag{2.6}$$

W_e is the effective width of the internal strip conductor defined as below [20]:

$$\frac{W_e}{h} = \frac{W}{h} - \begin{cases} 0 & , \ for \ \frac{W}{h} > 0.35 \\ (0.35 - W/h)^2 & , \ for \ \frac{W}{h} < 0.35 \end{cases} \tag{2.7}$$

Given $Z_0 = 50\Omega$, $h = 35mil$, ε_r=3.34, then solve the equations (2.6) and (2.7), we can get that $W = 20.65\ mil$. Since W solved by the equations is an approximate value, so fine tuning of the dimensions of the Stripline has been done to match the 50Ω characteristic impedance. The final dimensions of Stripline are shown in Table 2.2:

W	h	t
19.5 mil	35 mil	17.5 um

Table 2.2 Parameters of Stripline with 50Ω characteristic impedance.

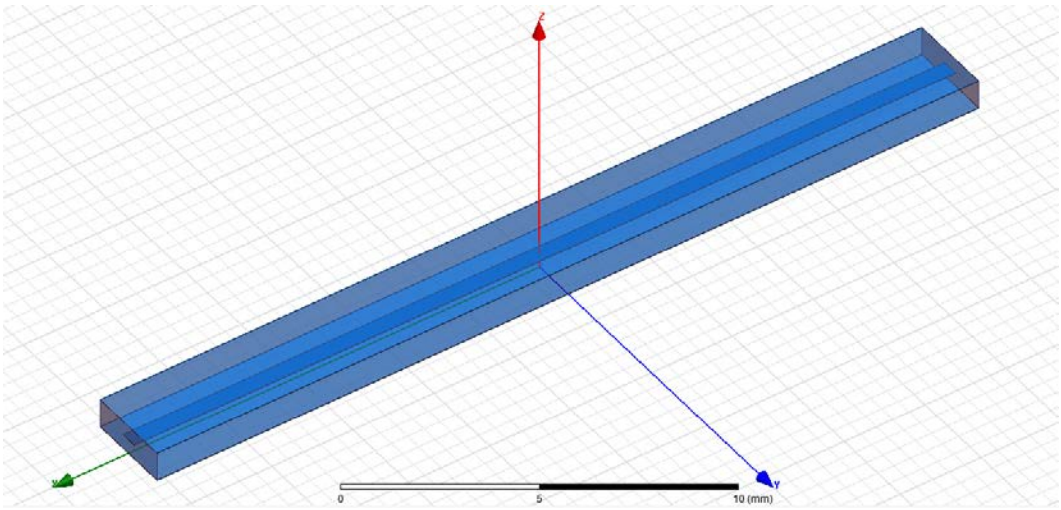

Figure 2.24 HFSS simulation model of Stripline.

The simulation model of Stripline is shown in Figure 2.24, and the simulation results for different operation bands are shown in Figure 2.25, Figure 2.26 and Figure 2.27, respectively.

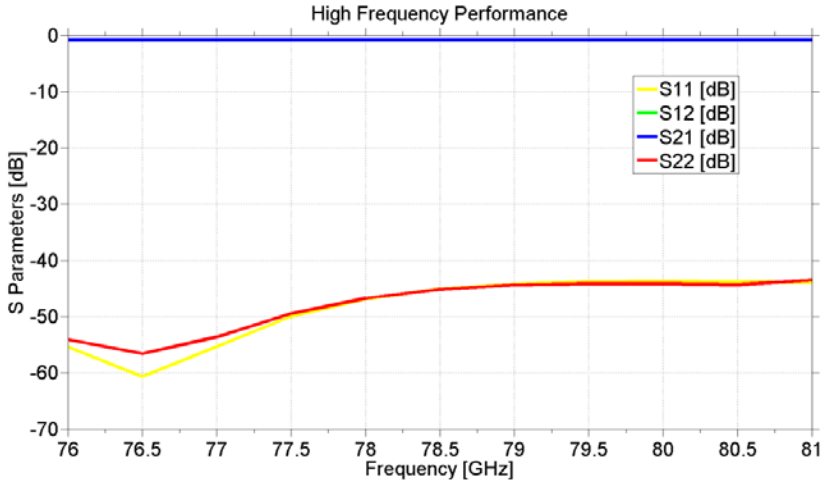

Figure 2.25 S-Parameters of Stripline for 76-81 GHz.

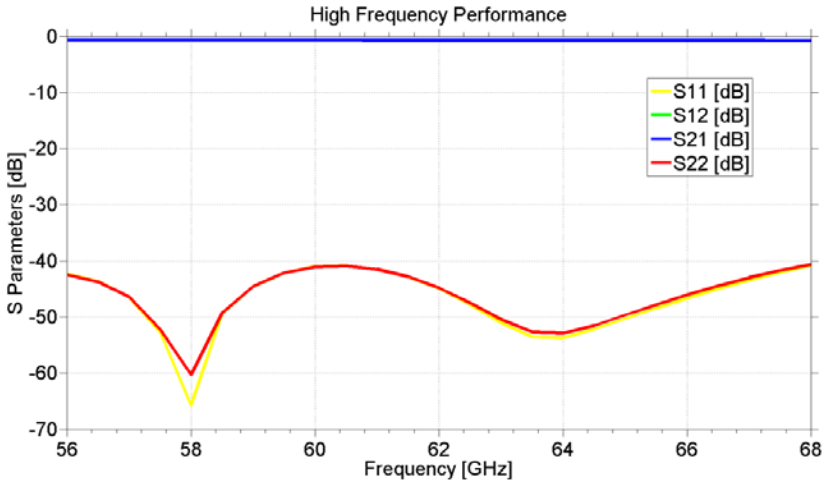

Figure 2.26 S-Parameters of Stripline for 56-68 GHz.

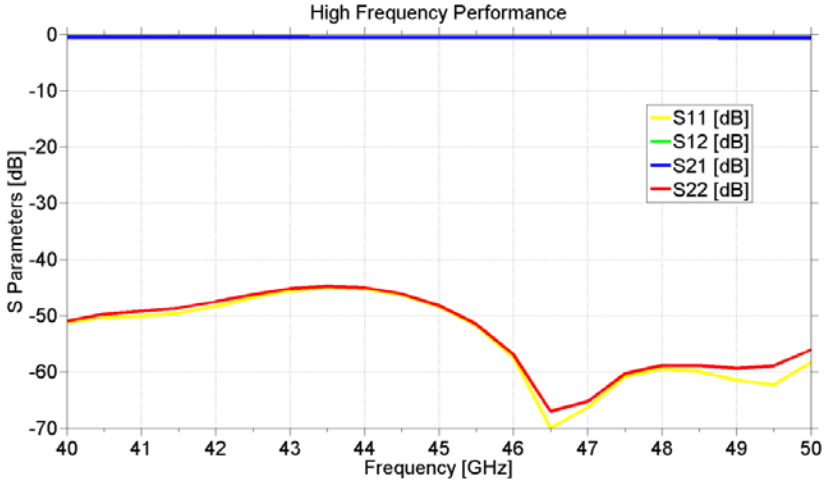

Figure 2.27 S-Parameters of Stripline for 40-50 GHz.

The striplines designed for different operation bands have shown good high frequency performance. The return loss of different-band striplines is all below -40 dB and the insertion loss is all above -0.8 dB in their respective operation bands.

2.2.3 Microstrip Design

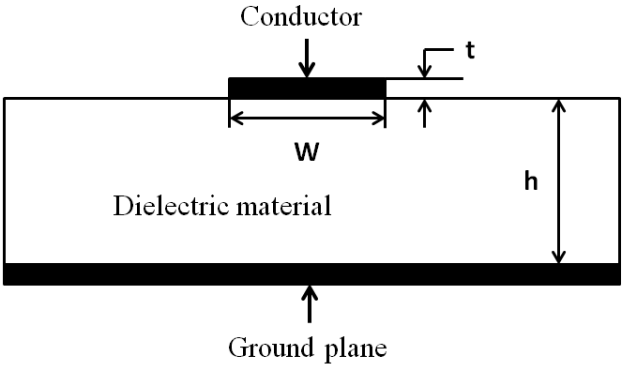

Figure 2.28 Microstrip cross-section.

Design 1 inch long 50Ω (characteristic impedance) Microstrip lines for the three different operation bands (76-81 GHz, 40-50 GHz, and 56-68 GHz). The Megtron 6 with dielectric constant ('ε_r') 3.34 and loss tangent ('$tan\delta$') 0.002 is selected as the dielectric material, and 0.5 oz. copper with conductivity ('σ') 5×10^7 S/m is selected as the metallic conductor and ground material, and the thickness "t" of conductor and ground plane is 17.5 um.

The Microstrip characteristic impedance can be defined as below [20]:

$$Z_0 = \frac{60}{\sqrt{\varepsilon}} \ln\left(\frac{8h}{W} + \frac{W}{4h}\right) (\Omega) \qquad \text{for } \frac{W}{h} \leq 1 \qquad (2.8)$$

$$Z_0 = \frac{120\pi}{\sqrt{\varepsilon}[\frac{W}{h} + 1.393 + 0.667\ln(\frac{W}{h} + 1.444)]} (\Omega) \qquad \text{for } \frac{W}{h} \geq 1 \qquad (2.9)$$

Since the dielectric height h is set as 35mil, ε is 3.34, and Z_0 is 50Ω, so according to equation (2.9), the width of the conductor W can be calculated as about 67mil. However the Microstrip characteristic impedance changes slightly with frequency [20], so fine tuning of the conductor width W should be done to match the 50Ω characteristic impedance for different operation bands.

The detailed dimensions of Microstrip for different bands are shown in Table 2.3:

Operation Bands	w	h	t
76-81 GHz	95 mil	35 mil	17.5 um
56-68 GHz	94 mil	35 mil	17.5 um
40-50 GHz	89 mil	35 mil	17.5 um

Table 2.3 Parameters of Microstrip for different operation bands.

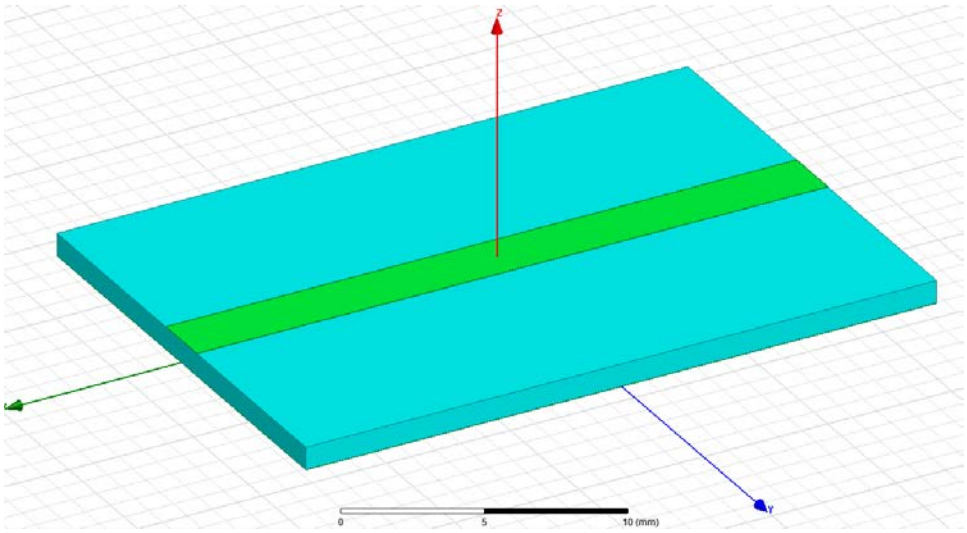

Figure 2.29 HFSS simulation model of Microstrip.

The simulation model of Microstrip is shown in Figure 2.29, and the simulation results for different operation bands are shown in Figure 2.30, Figure 2.31 and Figure 2.32, respectively.

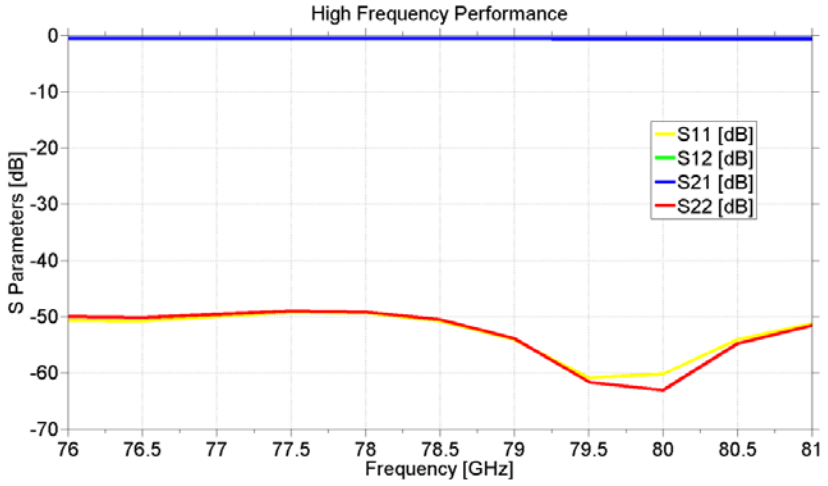

Figure 2.30 S-Parameters of Microstrip for 76-81 GHz.

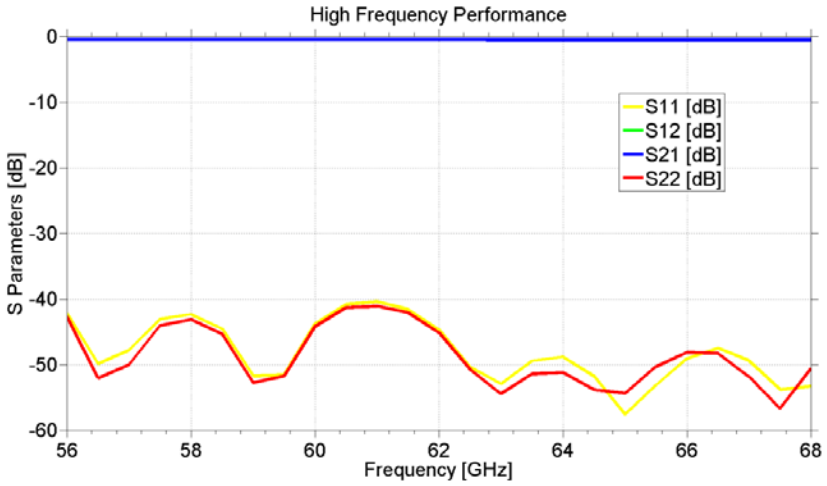

Figure 2.31 S-Parameters of Microstrip for 56-68 GHz.

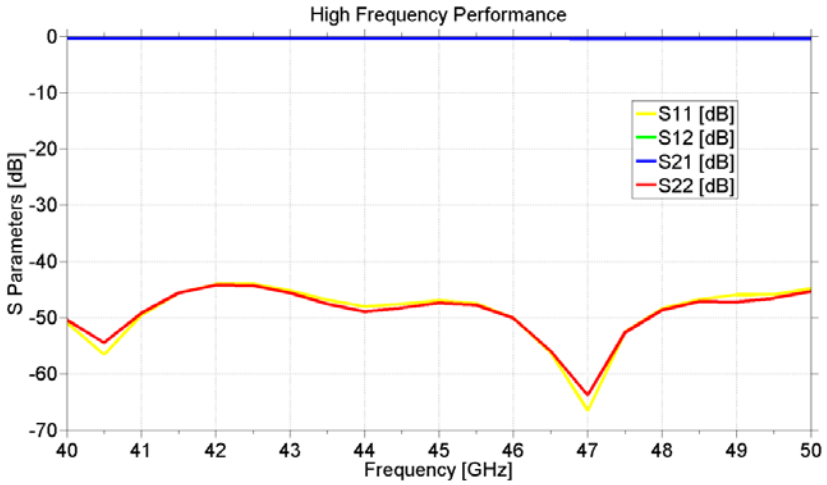

Figure 2.32 S-Parameters of Microstrip for 40-50 GHz.

For the Microstrips designed for different operation bands, the return loss is all below -40 dB and the insertion loss is all above -0.6 dB in their respective operation bands. The simulation results for Microstrips have shown very good high frequency performance.

2.2.4 GCPW Design

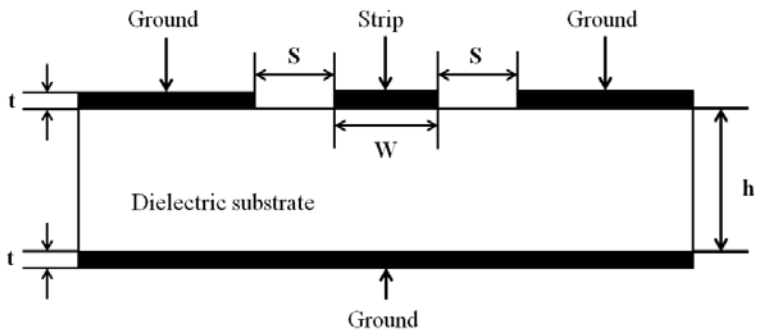

Figure 2.33 GCPW cross-section.

Design 1 inch long 50Ω (characteristic impedance) GCPW for the three different operation bands (76-81 GHz, 40-50 GHz, and 56-68 GHz). Similarly, select Megtron 6 ($\varepsilon_r = 3.34$, $tan\delta$=0.002) as the dielectric material, and select 0.5 oz. copper ($\sigma = 5 \times 10^7$ S/m) as the metallic conductor and ground material, and the thickness "t" of conductor and ground plane is 17.5 um.

The GCPW characteristic impedance can be defined as below [21, 22]:

$$Z_0 = \frac{60\pi}{\sqrt{\varepsilon_{eff}}} \frac{1}{\frac{K(k)}{K(k\prime)} + \frac{K(kl)}{K(kl\prime)}} \tag{2.10}$$

And

$$k = W/(W + 2 * S);$$

$$k' = \sqrt{1 - k^2};$$

$$kl' = \sqrt{1 - kl^2}; \tag{2.11}$$

$$kl = \frac{\tanh(\frac{\pi a}{4h})}{\tanh(\frac{\pi b}{4h})};$$

$$\varepsilon_{eff} = \frac{1 + \varepsilon_r \frac{K(k\prime)\,K(kl)}{K(k)\,K(kl\prime)}}{1 + \frac{K(k\prime)\,K(kl)}{K(k)\,K(kl\prime)}};$$

In equation 2.10, $K(k)$, $K(k')$, $K(kl)$ and $K(kl')$ represent the complete elliptic integral of the first kind and its complement.

Since the characteristic impedance is 50Ω, and set the conductor width W as 50mil, we can use the equations above to get the value of gap width S between the strip and ground conductors. However, the calculation is not accurate enough; fine tuning of the gap width S should be done to match the 50Ω characteristic impedance for different operation bands.

The detailed dimensions of GCPW for different bands are shown in Table 2.4:

Operation Bands	W	S	t	h
76-81 GHz	10 mil	1.5 mil	17.5 um	35mil
56-68 GHz	11 mil	2 mil	17.5 um	35mil
40-50 GHz	16 mil	2 mil	17.5 um	35mil

Table 2.4 Parameters of GCPW for different operation bands.

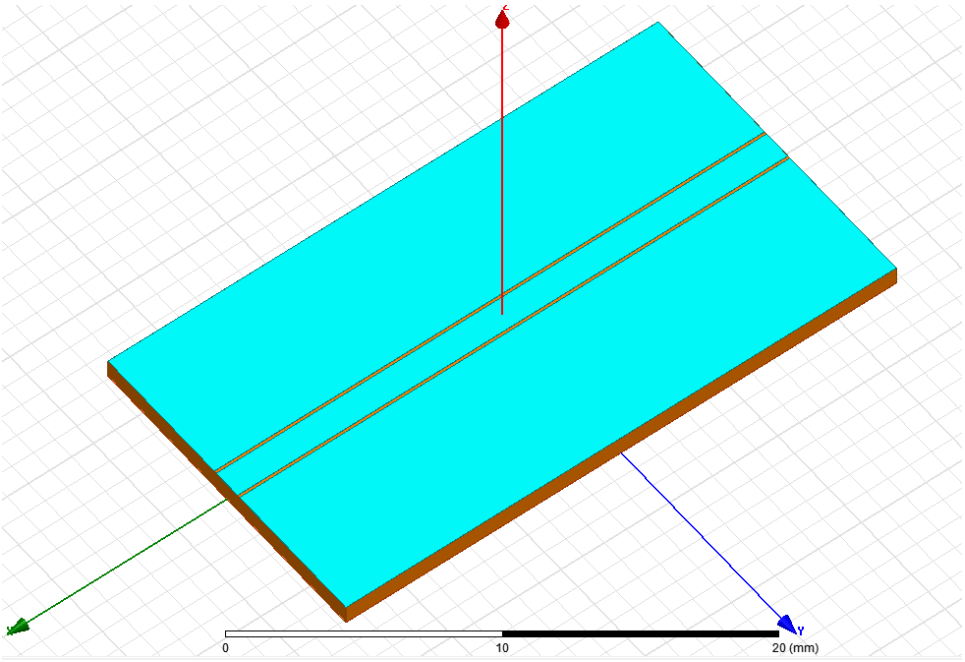

Figure 2.34 HFSS simulation model of GCPW.

The simulation model of GCPW is shown in Figure 2.34, and the simulation results for different operation bands are shown in Figure 2.35, Figure 2.36 and Figure 2.37, respectively.

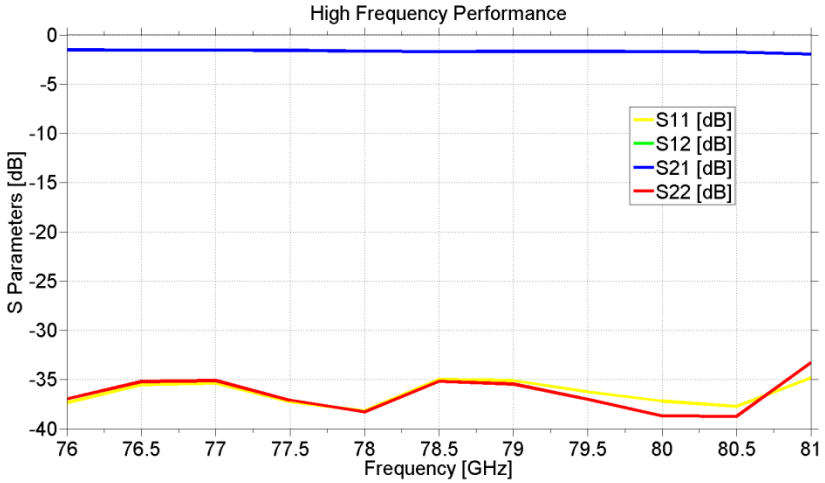

Figure 2.35 S-Parameters of GCPW for 76-81 GHz.

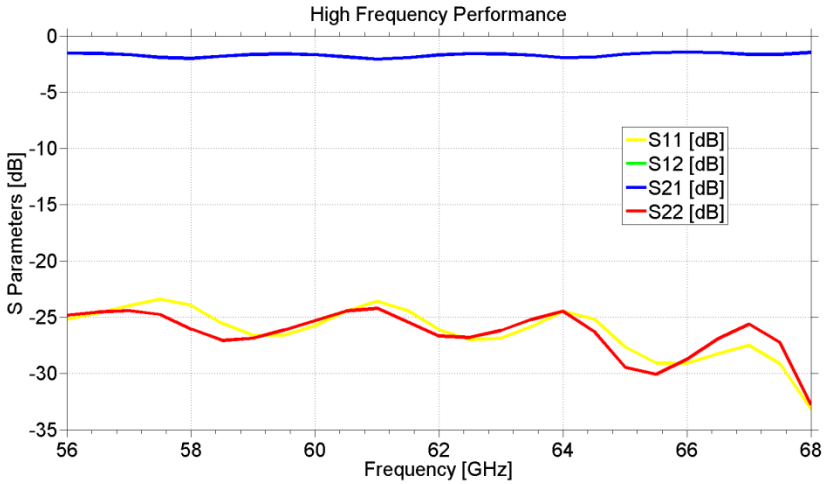

Figure 2.36 S-Parameters of GCPW for 56-68 GHz.

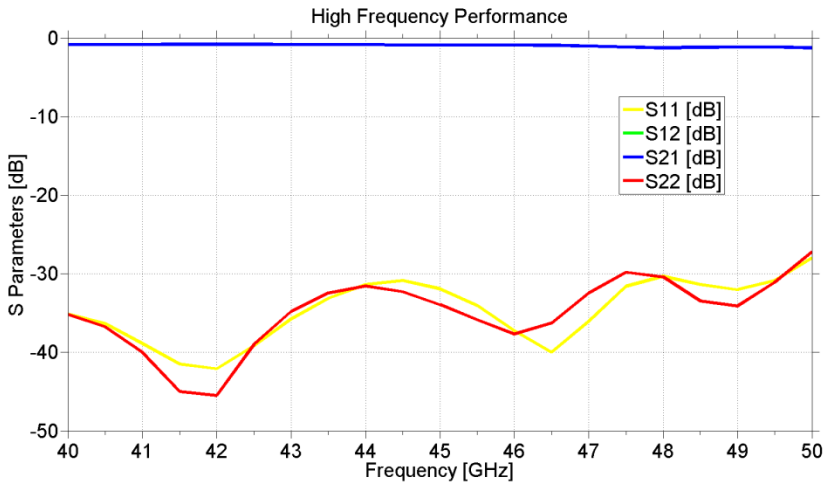

Figure 2.37 S-Parameters of GCPW for 40-50 GHz.

For the GCPW designed for different operation bands, the return loss is all below -24 dB and the insertion loss is all above -2 dB. Since the substrate thickness is fixed at 35 mil and is much larger than the gap width, more radiation loss is caused for GCPW than for the other transmission lines.

2.3 Comparison between SIW and other T-lines

Based on the designs and simulations of various transmission lines, we will make comparison of them from the following several aspects, which can help us to better learn about the advantages and disadvantages of SIW:

- **Planar Nature**

Firstly from the aspect of structure geometry, SIW has the same planar nature as Stripline, Microstrip and GCPW, thus it is easy to be integrated with other planar components or circuits. However, RWG do not have planar nature and are relatively bulky compared to the SIW.

- **Relatively Low Loss**

Compared with RWG, SIW has higher insertion loss, for the RWG is air-filled, while SIW is dielectric-filled, which will cause considerable dielectric loss. Constrained by the project requirements, the substrate material of SIW is selected as Megtron 6 with loss tangent 0.002. However, if another dielectric material with lower loss tangent was selected for SIW, the dielectric loss would be much smaller.

Compared with Stripline, Microstrip with the same substrate, the insertion loss of SIW is comparable. As the working frequency band gets higher, there will be more insertion loss caused for SIW. However, compared with GCPW with the same dielectric, GCPW has much more insertion loss than SIW and other T-lines. Since the gap between the trace and returning conductors of GCPW should be very small to support electric fields primarily concentrated in dielectric, and the dielectric substrate thickness should also be small (which usually set as twice the gap width) to minimize radiation [20], the fixed substrate thickness (35 mil) is too large compared to the gap width (2 mil), which caused much radiation loss.

- **Mutual Electromagnetic Isolation**

When integrated in the same circuit board, the distance between transmission lines such as stripline, microstrip or GCPW should exceed a specific value to avoid the mutual electromagnetic coupling or interference. However, for the relatively enclosed structure like RWG, there are no such considerations needed for the SIW circuit design.

Here, two adjacent SIW lines in parallel are designed and simulated to verify the mutual electromagnetic isolation property of SIW. The 1 inch long V-band SIW lines are modeled in two situations, one situation is that the two SIW lines have one row of vias in common, and another situation is the two SIW are located in parallel with a distance 25 mil between them. The simulation models are shown in Figure 2.38 (a) and Figure 2.38 (b), respectively.

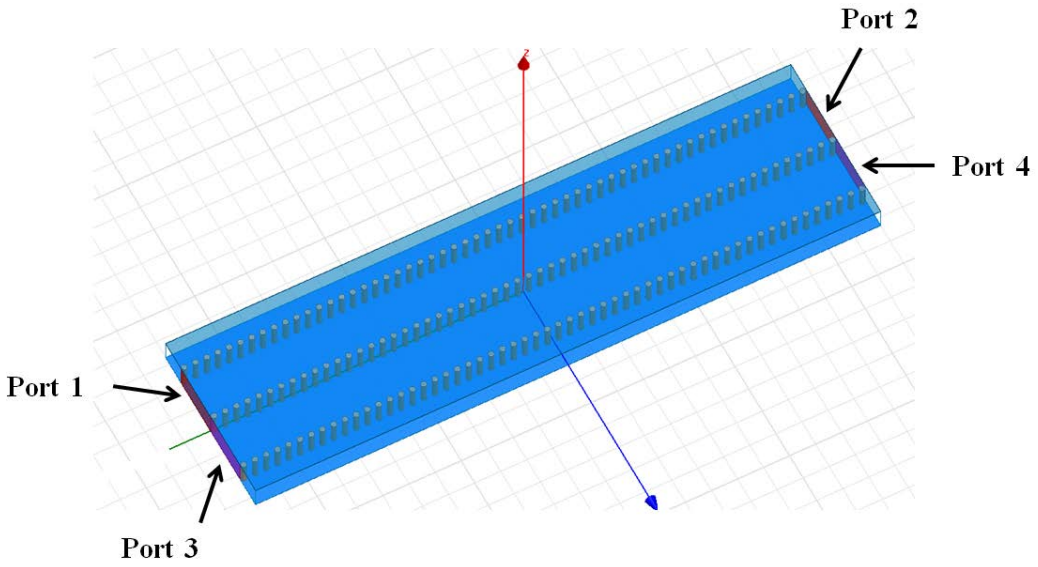

Figure 2.38 (a) Simulation model of two SIW lines with one row of vias in common.

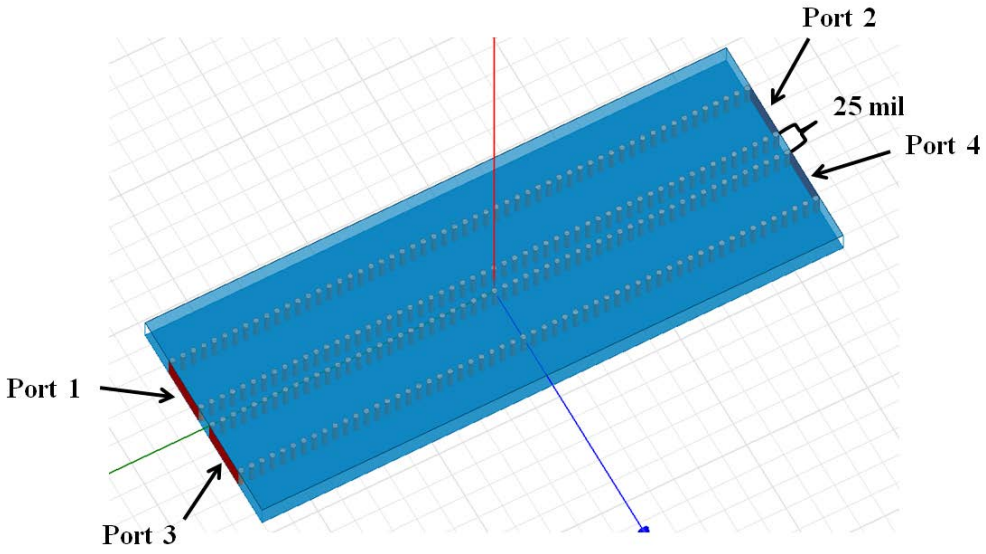

Figure 2.38 (b) Simulation model of two SIW lines in parallel.

From the HFSS simulated S parameters (which are shown Figure 2.39 (a) and Figure 2.39 (b)) and E-field plots (which are shown in Figure 2.40 (a) and Figure 2.40 (b)), we can see the good isolation characteristics of SIW.

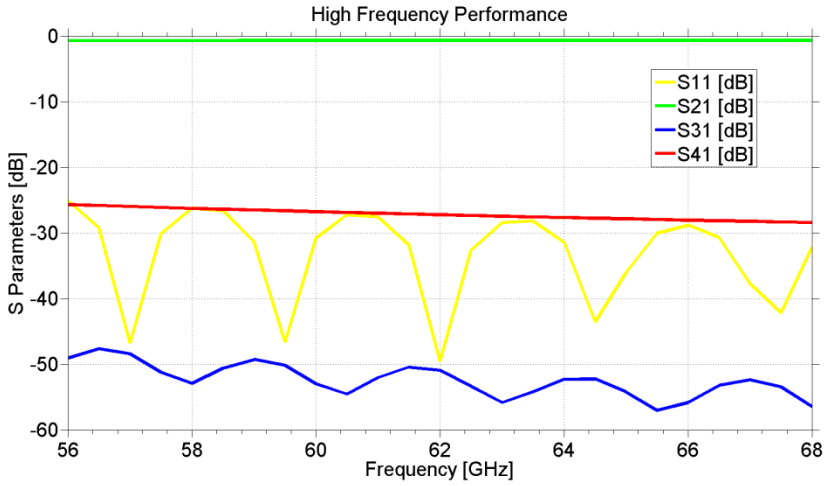

Figure 2.39 (a) S parameters of two SIW lines with one row of vias in common.

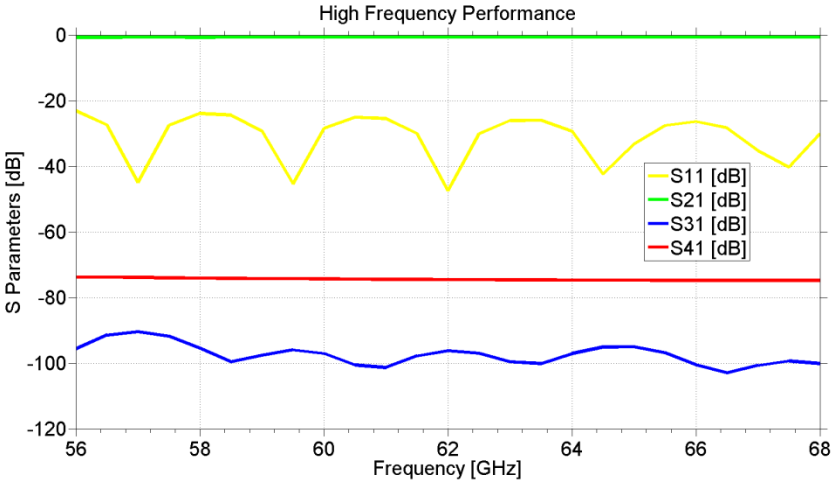

Figure 2.39 (b) S parameters of two SIW lines in parallel.

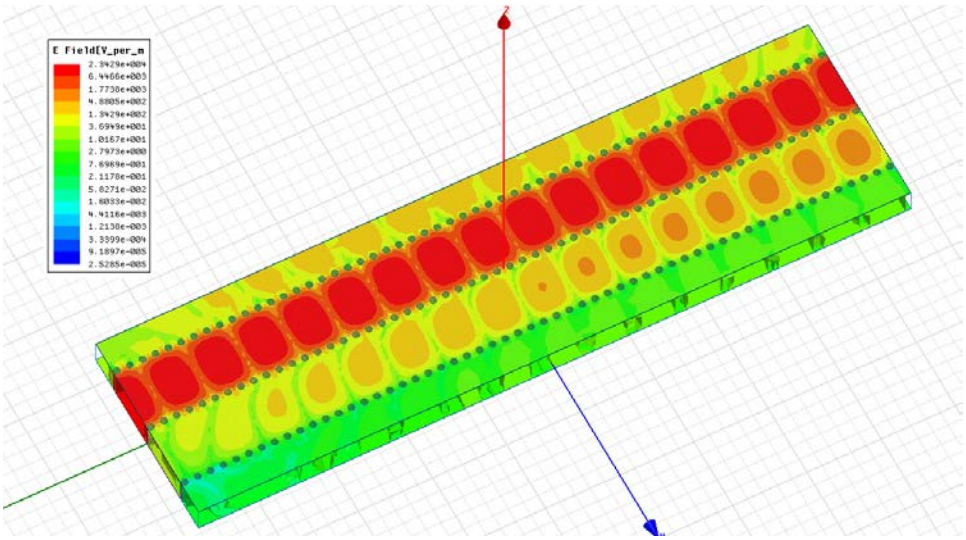

Figure 2.40 (a) E-field plot at 68 GHz of two SIW lines with one row of vias in common.

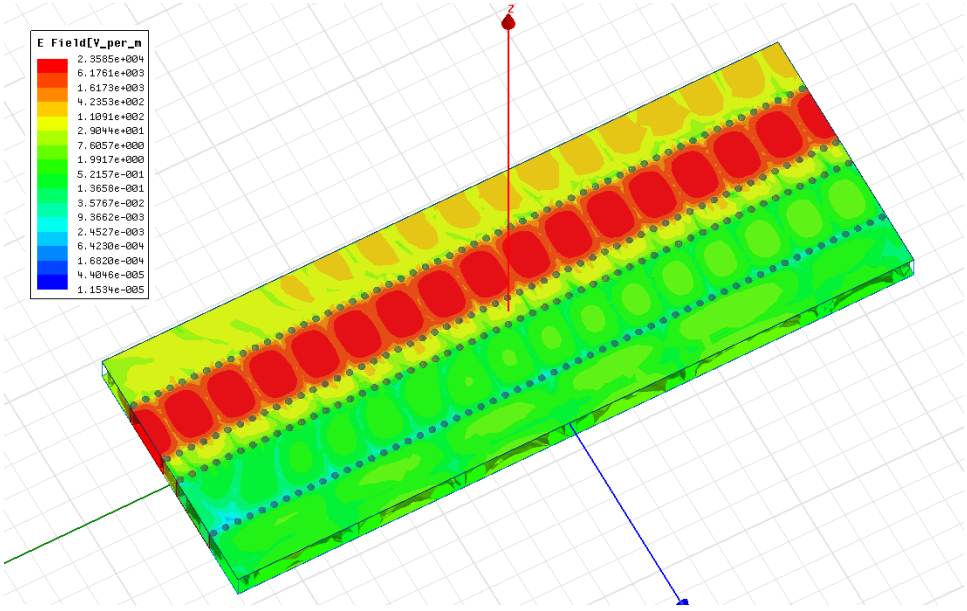

Figure 2.40 (b) E-field plot at 68 GHz of two SIW lines in parallel.

From the simulation results, the isolation (S31 and S41) between the two SIW lines with a common row of vias at 68 GHz is lower than -25 dB, and the isolation between the parallel two SIW lines at 68 GHz is lower than -70 dB. The sufficient electromagnetic isolation is an obvious advantage for SIW to be integrated in mm-wave circuits.

Chapter 3

Transition Design between SIW and RWG

From the previous chapter, we can see that rectangular waveguides have better power handling capability and more structure rigidity compared to SIW, and they do not have any mutual electromagnetic interference compared to the other transmission lines since rectangular waveguides are enclosed structures. Thus the hybrid design of planar transmission lines and RWG could be inevitable [11]. In this chapter, the transitions between SIW and RWG working for different operative bands are described. The transition structures, design process, high frequency performance and analysis are presented in detail.

3.1 Slot Transition Design for Narrow Band

A coupling slot etched on the metal layer of the SIW as the transition between SIW and RWG realized at 35 GHz is proposed in [11], and this kind of transition structure is adopted and explored for operation band 76-77 GHz in this thesis.

3.1.1 Design Strategy and Initial Conditions

As shown in Figure 3.1 [11], the rectangular waveguide (RWG) can surface-mounted to the SIW by screwing the flanges, and the electromagnetic energy can be coupled from RWG to SIW through the slot etched on the metallic layer of SIW; A row of vias is placed at one end of the SIW line to form a short circuit [11].

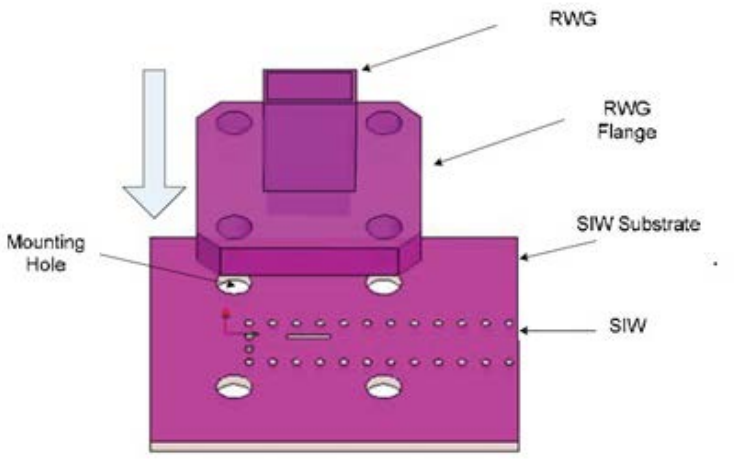

Figure 3.1 Slot transition between RWG and SIW [11].

In order to get a good impedance matching between SIW and RWG, the dimension and position of the slot etched play an important role [11]. As shown in Figure 3.2, L is the length of the slot, w is the width of the slot, a is the center to center distance between the row of vias at the end of SIW and the etched slot, and b is the centerline to centerline offset from the slot to SIW.

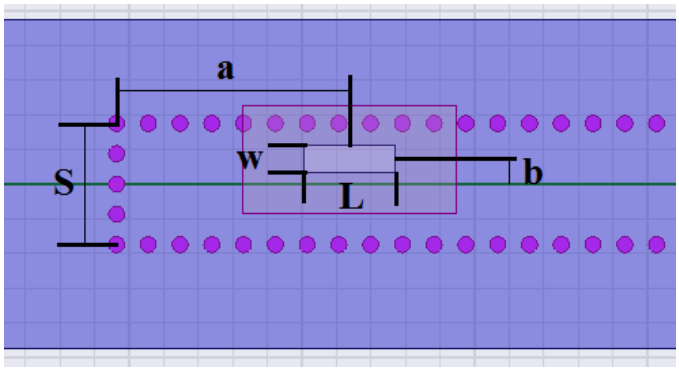

Figure 3.2 Dimensions of the slot transition between RWG and SIW.

There are some basic design rules for this kind of slot transition to follow as below [11]:

$$a = (2n + 1) \times \frac{1}{4}\boldsymbol{\lambda}, \qquad n = 0,1,2,3 \ldots$$

$$L = \frac{1}{2} \times \boldsymbol{\lambda} \tag{3.1}$$

$$b = \frac{1}{4} \times S$$

Here, λ is the wavelength at the central frequency, and S is the center-to-center distance between the two rows of vias in SIW. In my design, the distance a between the short circuit and the slot center is chosen as 3 times of quarter-wavelength. However the rules above can only be used as the initial conditions for the dimension and position of the slot etched, optimization of the dimension and position of the slot needs to be done in order to get proper impedance matching.

3.1.2 Transition Design and Simulation for 76-77 GHz

The design and simulation model of the transition between RWG and SIW for 76-77 GHz is shown in Figure 3.3. Since the 76-77 GHz belongs to the E band range (60 GHz to 90 GHz), the RWG is selected as standard WR12, which has the inner dimensions of $0.122\,inch \times 0.061\,inch$ ($3.0988\,mm \times 1.5494\,mm$). The height of the standard RWG does not affect the high frequency performance of the transition, so the height of WR12 is set as 1cm in the simulation. The dimensions of the SIW are kept as the same as the dimensions of the E-band SIW described in chapter 2, and the length of the core SIW is 1 inch.

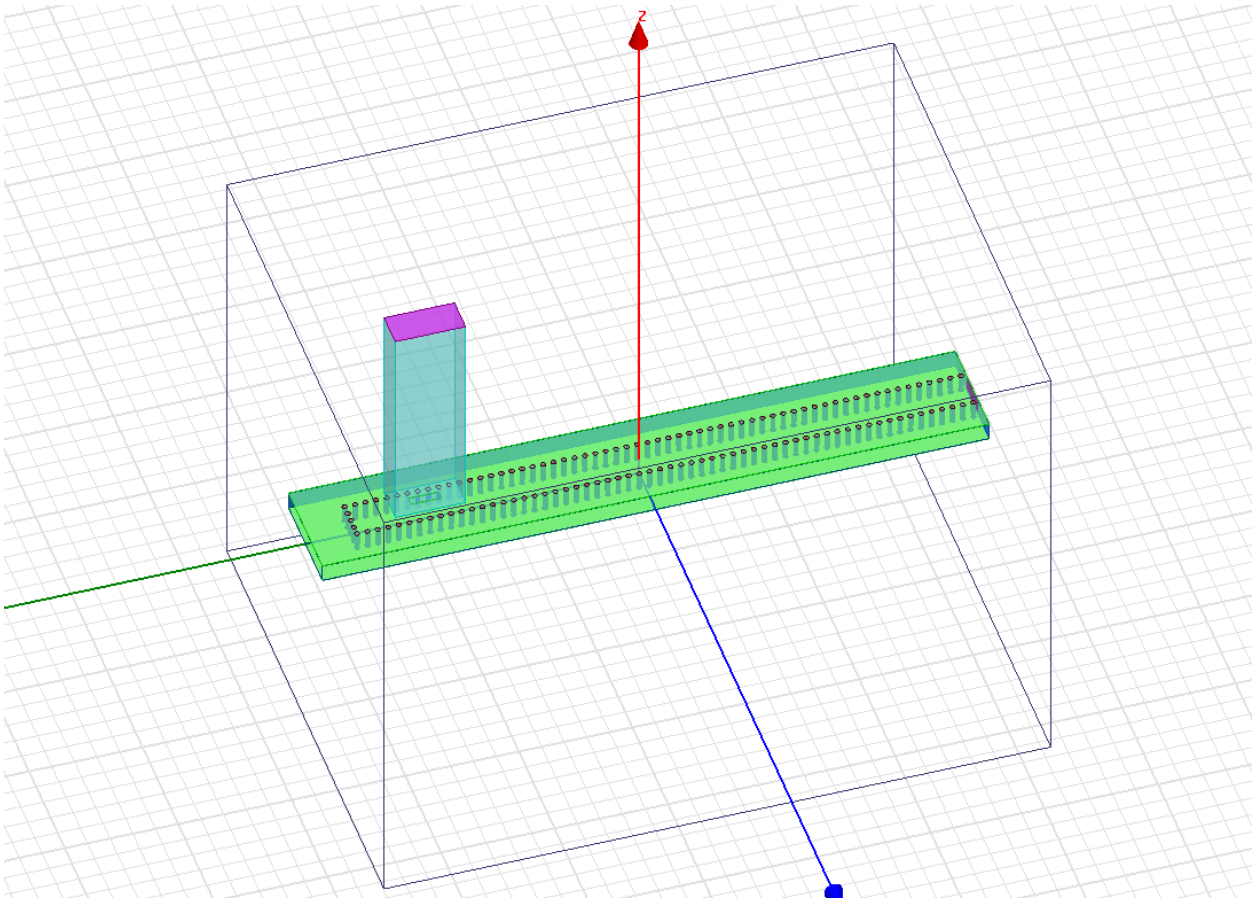

Figure 3.3 HFSS simulation model of the slot transition between RWG and SIW.

After optimization, the dimensions and position of the slot transition from RWG to SIW are shown in Table 3.1:

a (mil)	L (mil)	w (mil)	b (mil)
95.75	51.5	11	19

Table 3.1 Dimensions of the slot transition between RWG and SIW.

The simulated reflection coefficients (return loss) and transmission coefficients (insertion loss) are shown in Figure 3.4 and Figure 3.5, respectively.

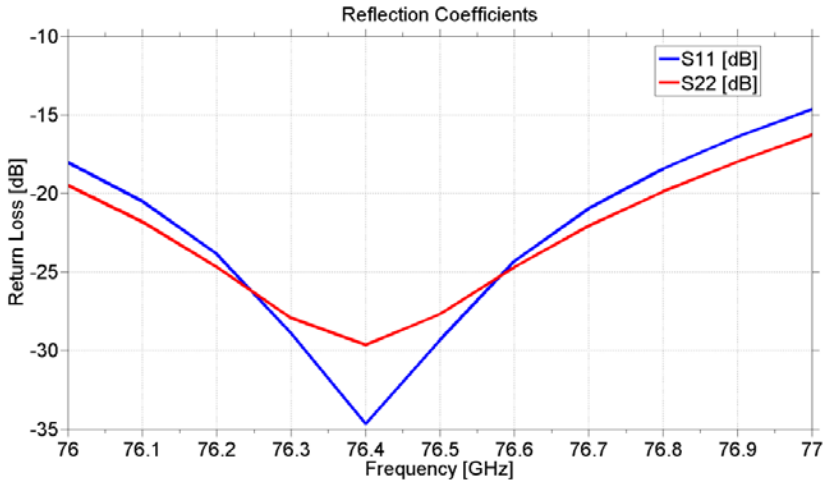

Figure 3.4 The reflection coefficients (return loss) of the slot transition between RWG and SIW for 76-77GHz.

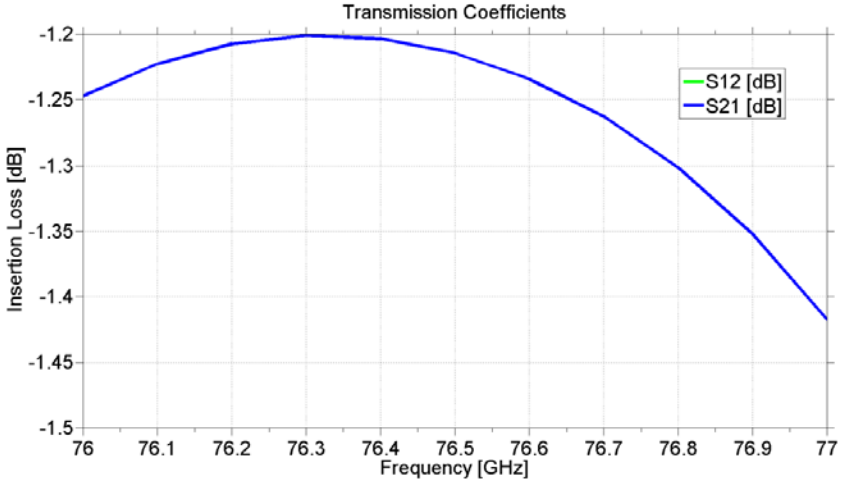

Figure 3.5 The transmission coefficients (insertion loss) of the slot transition between RWG and SIW for 76-77 GHz.

The simulation results of the slot transition shows return loss less than -14.6 dB and insertion loss more than -1.45 dB over the whole frequency range from 76 GHz to 77 GHz. Since this kind of transition exhibits good high frequency performance, and can be fabricated with traditional printed circuit board (PCB) technologies, it could be widely used in the hybrid design of SIW and RWG for narrow operation bands [11].

3.1.3 Slot Transition Loss Extraction

Since the simulation structures include RWG, slot transition and SIW, the simulated return loss and insertion loss are the total loss caused by all of them. How to get the loss only caused by slot transition? Here the method of numerical fitting is adopted to extract the loss of transition portion. That is by simulating the whole structures (RWG-transition-SIW) with different lengths of core SIWs, such as 0.5 inch, 1 inch and 2 inch, while the RWG and the transitions are kept identical, then extract the return and insertion loss at specific frequency, make the best fitting line to get the loss of the transition portion. The loss caused by the RWG portion is so small that is ignored here.

The simulation models (top view) of the RWG-transition-SIW with different-length SIWs are shown in Figure 3.6 as below:

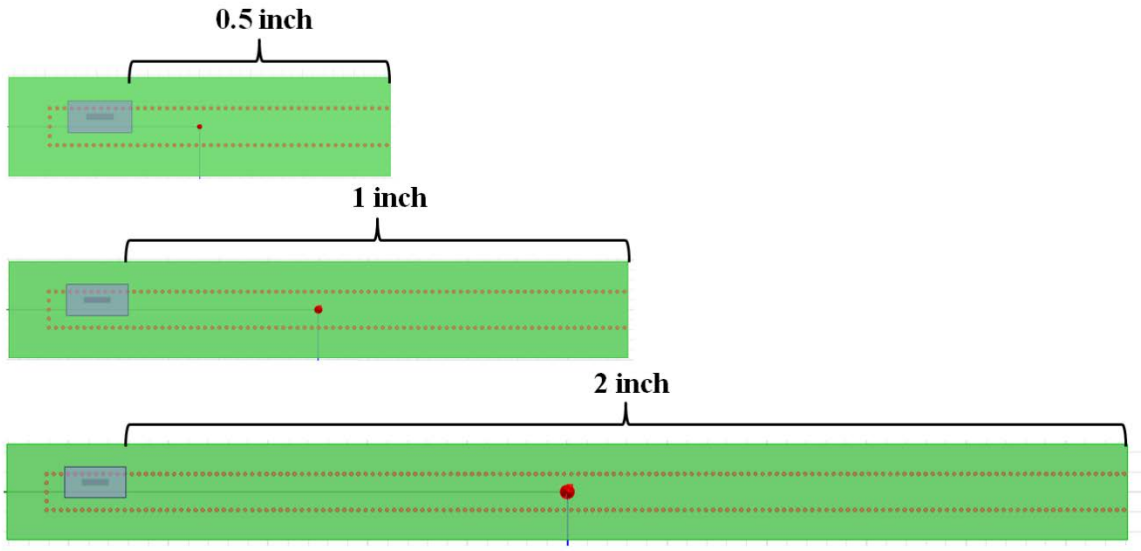

Figure 3.6 The simulation models (top view) of RWG-transition-SIW structure with different-length core SIWs.

The simulation results for the whole structures with 0.5 inch long and 2 inch long core SIWs are shown in Figure 3.7 and Figure 3.8, respectively.

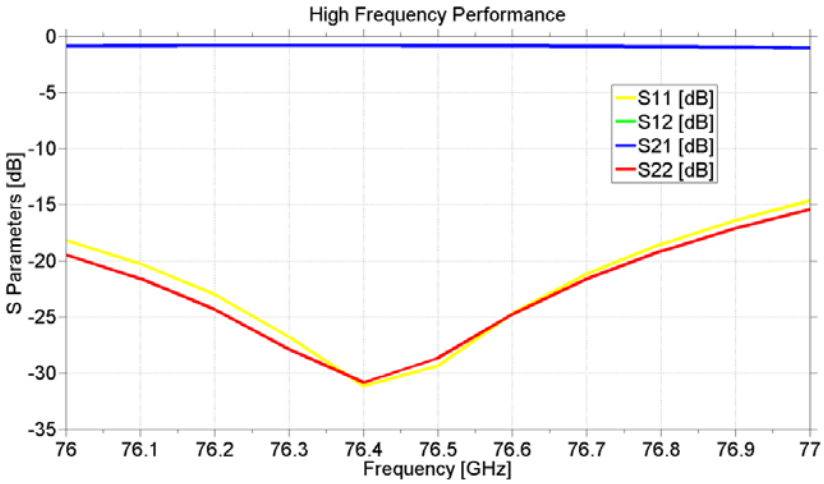

Figure 3.7 S parameters of the whole structure with 0.5 inch long core SIW.

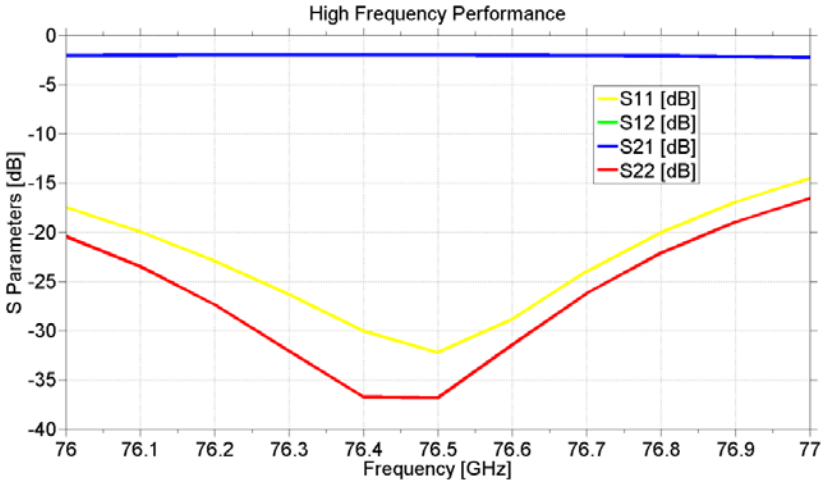

Figure 3.8 S parameters of the whole structure with 2 inch long core SIW.

Here, we mainly concern the return loss S11 and insertion loss S21 at the central frequency and border frequencies. The simulated data for the whole structure with different-length core SIWs at these specific frequencies are shown in Table 3.2.

S11 / S21	0.5 inch	1 inch	2 inch

@ 76 GHz	-0.851 dB -18.162 dB	-1.247 dB -18.028 dB	-2.044 dB -17.451 dB
@ 76.5 GHz	-0.826 dB -29.365 dB	-1.214 dB -29.334 dB	-1.995 dB -32.197 dB
@ 77 GHz	-1.029 dB -14.636 dB	-1.417 dB -14.647 dB	-2.228 dB -14.497 dB

Table 3.2 The return loss and insertion loss of RWG-transition-SIW structures for different-length core SIWs at 76 GHz, 76.5 GHz and 77 GHz.

According to the simulated data, make the best fitting lines and extract the insertion loss and return loss of the transition portion, which are shown in Figure 3.9 and Figure 3.10, respectively.

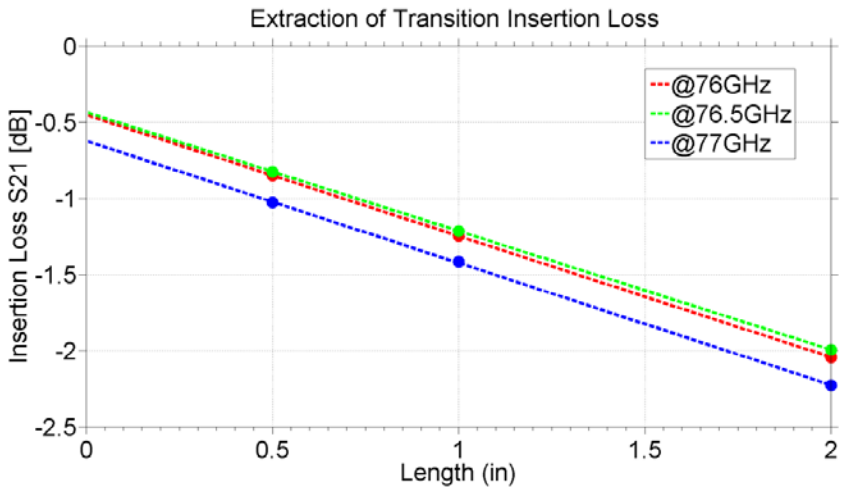

Figure 3.9 Insertion loss fitting and extraction for transition portion.

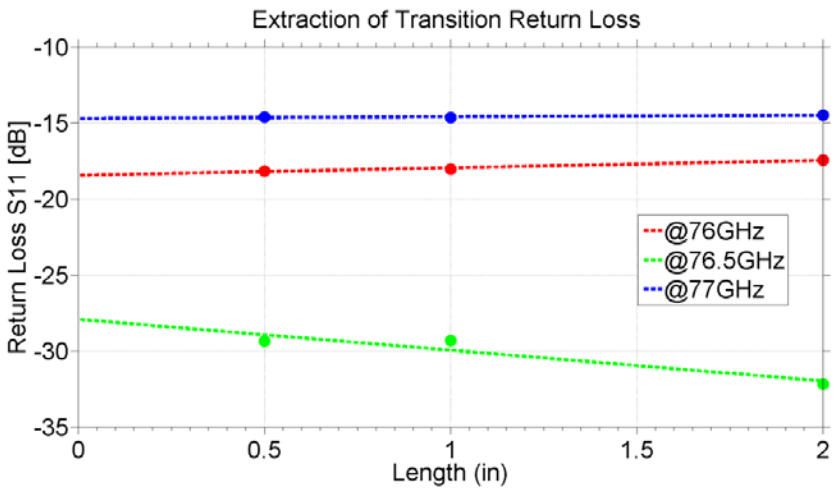

Figure 3.10 Return loss fitting and extraction for transition portion.

According to the fitting lines, we can calculate and get the loss of the transition portion (when Length = 0 inch) shown in Table 3.3 as below:

	@ 76 GHz	@ 76.5 GHz	@ 77 GHz
Insertion Loss	-0.4525 dB	-0.4355 dB	-0.6235 dB
Return Loss	-18.4505 dB	-27.9335 dB	-14.7110 dB

Table 3.3 Slot transition loss at specific frequencies.

3.2 Aperture Transition Design for Broad Band

Though the slot transition between RWG and SIW described in chapter 3.1 has very good high frequency performance, the operative bandwidth is limited. For broad working band, other alternative of transition needs to be designed.

3.2.1 Transition Design and Simulation for 77-81 GHz, 56-68 GHz and 40-50 GHz

Another kind of aperture transition between RWG and SIW are proposed in [14], similarly to the slot transition proposed in chapter 3.1, a rectangular aperture was etched on one metallic

layer of the SIW. The RWG and core SIW do not change, however the differences include the dimension and position of the aperture between RWG and SIW, as well as the enlarged interface part of the SIW with the RWG. As shown in Figure 3.11, the whole structure (including the RWG, aperture and SIW) is symmetric on the central axis of the SIW. The SIW is shorted at one end by additional row of vias, and the width of the SIW gets wider around the aperture than the width of core SIW.

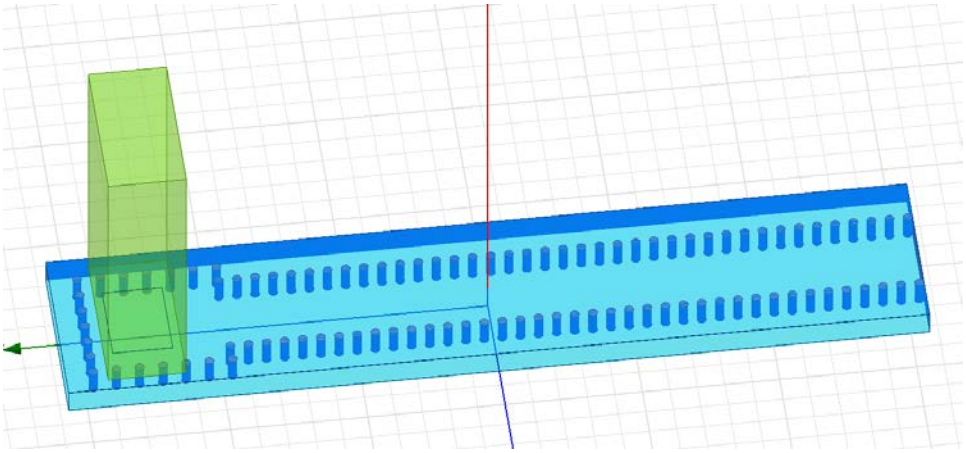

Figure 3.11 HFSS simulation model of aperture transition between RWG and SIW.

As shown in Figure 3.12, W is the width of the aperture, L is the length of the aperture, S is the center-to-center distance between the row of vias as the shorted circuit and the aperture, c is the length of the enlarged end of SIW, and a is the width of the enlarged end of SIW.

For the high frequency performance of aperture transition, L, S and c mainly determine the central frequency of working bands, while the reflection coefficients have correlation with W and a. All of these parameters interact with each other, and they together determine the energy coupling effect between RWG and SIW. Optimization needs to be done to get a good impedance matching between RWG and SIW.

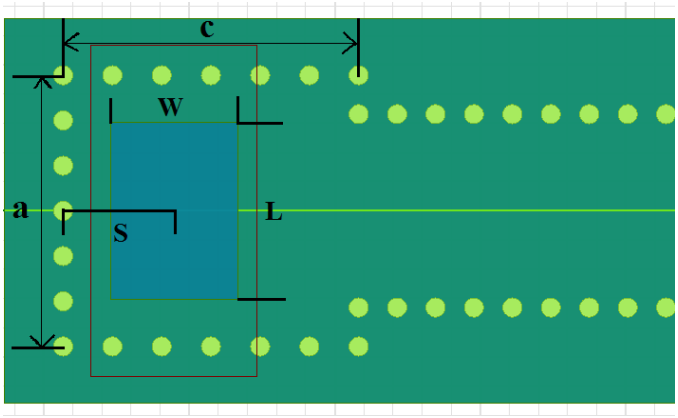

Figure 3.12 Dimensions of the aperture transition between RWG and SIW.

The aperture transitions have been designed for three different operative bands, including 77-81 GHz (E band), 56-68 GHz (V band), and 40-50 GHz (Q band). For 77-81 GHz, the core SIW adopts the same E band SIW dimensions described in Chapter 2, and the RWG is selected as WR12 with inner dimensions of $0.122\ inch \times 0.061\ inch$ ($3.0988\ mm \times 1.5494\ mm$); For 56-68 GHz, the core SIW adopts the same V band SIW dimensions described in Chapter 2, and the RWG is selected as WR15 with inner dimensions of $0.148\ inch \times 0.074\ inch$ ($3.7592\ mm \times 1.8796\ mm$); For 40-50 GHz, the core SIW adopts the same Q band SIW dimensions described in Chapter 2, and the RWG is selected as WR22 with inner dimensions of $0.224\ inch \times 0.112\ inch$ ($5.6896\ mm \times 2.8448\ mm$). The lengths of the core SIWs are all 1 inch long for different operative bands. After optimization, the final structure dimensions for these different bands are shown in Table 3.4 as below.

	W (mil)	L (mil)	S (mil)	c (mil)	a (mil)
77-81 GHz	44	47	42	102	115
56-68 GHz	50	70	115	196	122
40-50 GHz	86	120	75	200	183

Table 3.4 Dimensions of the aperture transitions between RWG and SIW for different operative bands.

The reflection coefficients (return loss) and transmission coefficients (insertion loss) of the aperture transition for 77-81 GHz are shown in Figure 3.13 and Figure 3.14, respectively. The simulation results show the return loss less than -10 dB and insertion loss more than -1.5 dB over the whole frequency range from 77 GHz to 81 GHz.

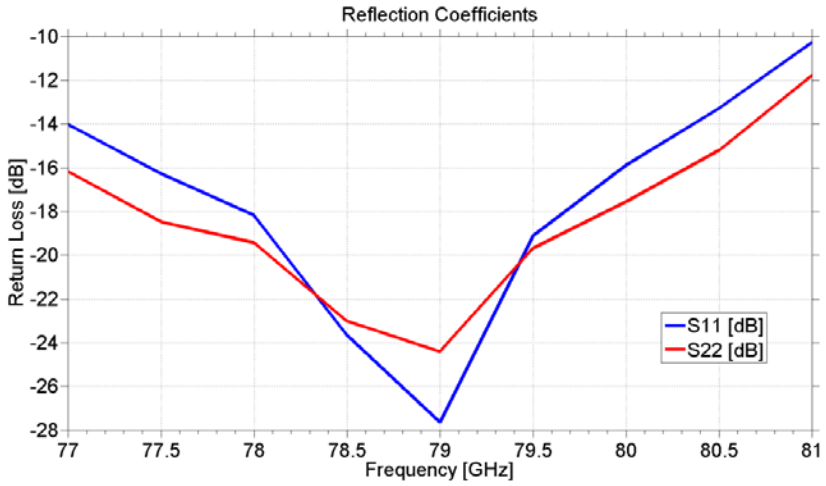

Figure 3.13 Return loss of the aperture transition between RWG and SIW for 77-81 GHz.

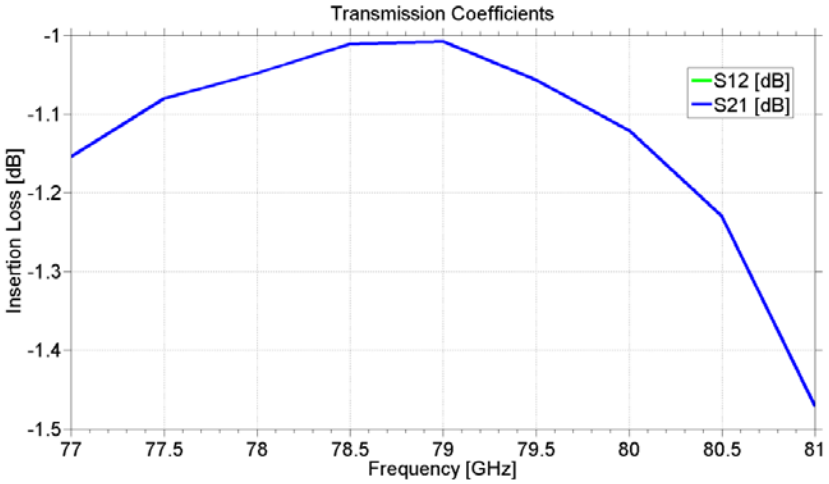

Figure 3.14 Insertion loss of the aperture transition between RWG and SIW for 77-81 GHz.

The reflection coefficients (return loss) and transmission coefficients (insertion loss) of the aperture transition for 56-68 GHz are shown in Figure 3.15 and Figure 3.16 respectively. The simulation results show the return loss less than -8.5 dB and insertion loss more than -1.5 dB over the whole frequency range from 56 GHz to 68 GHz.

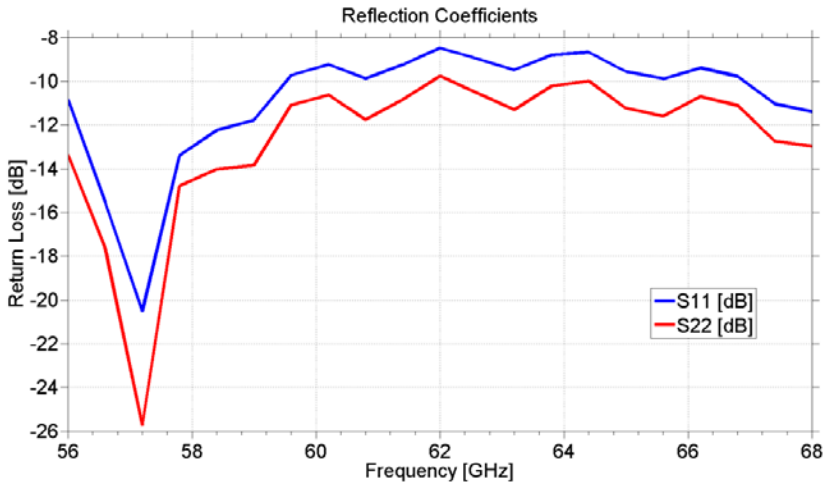

Figure 3.15 Return loss of the aperture transition between RWG and SIW for 56-68 GHz.

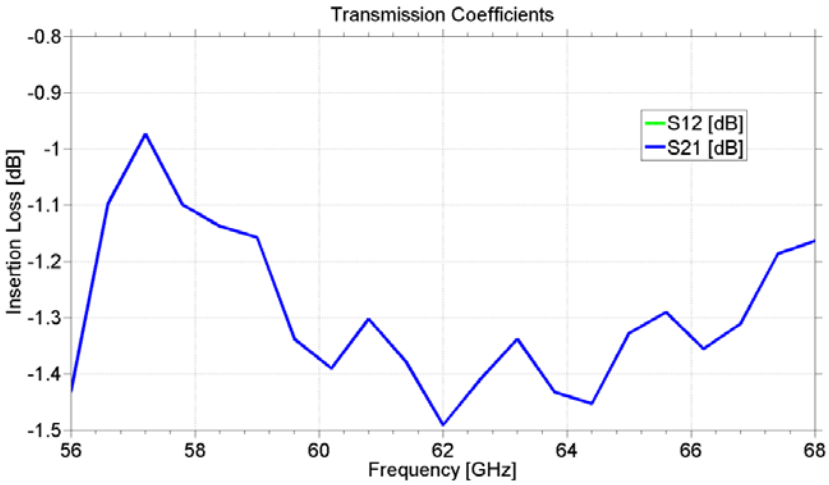

Figure 3.16 Insertion loss of the aperture transition between RWG and SIW for 56-68 GHz.

The reflection coefficients (return loss) and transmission coefficients (insertion loss) of the aperture transition for 40-50 GHz are shown in Figure 3.17 and Figure 3.18, respectively. The

simulation results show the return loss less than -9.5 dB and insertion loss more than -1.2 dB over the whole frequency range from 40 GHz to 50 GHz.

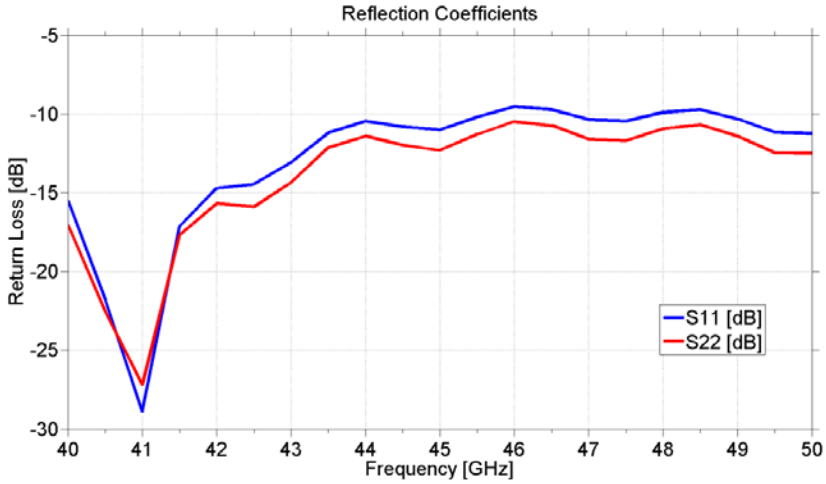

Figure 3.17 Return loss of the aperture transition between RWG and SIW for 40-50 GHz.

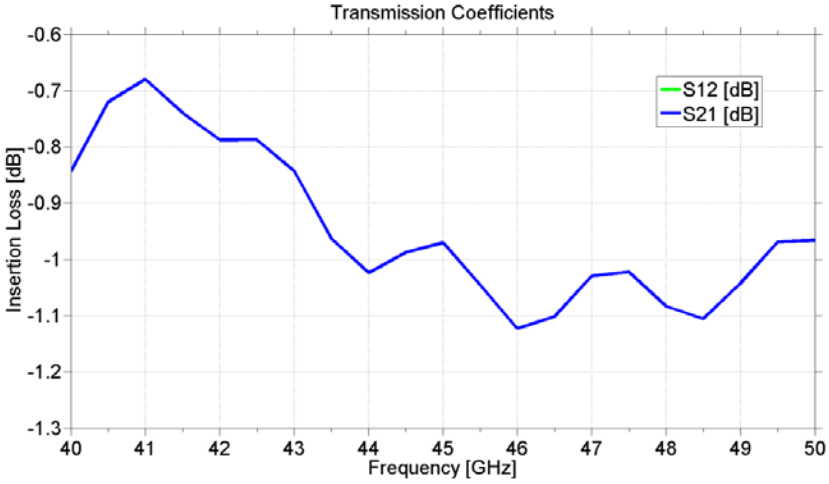

Figure 3.18 Insertion loss of the aperture transition between RWG and SIW for 40-50 GHz.

3.2.2 Aperture Transition Loss Extraction

Similarly use the method of numerical fitting to extract the loss of aperture transition portion for different operative bands. Change the lengths of core SIWs as 0.5 inch, 1 inch and 2 inch, while the RWG and transitions are kept unchanged, then extract the return and insertion loss at

specific frequencies, make the best fitting lines to get the loss of transition portions. Here the loss caused by RWG portion is ignored for it is too small.

The HFSS simulation models (top view) with different-length core SIWs are shown in Figure 3.19.

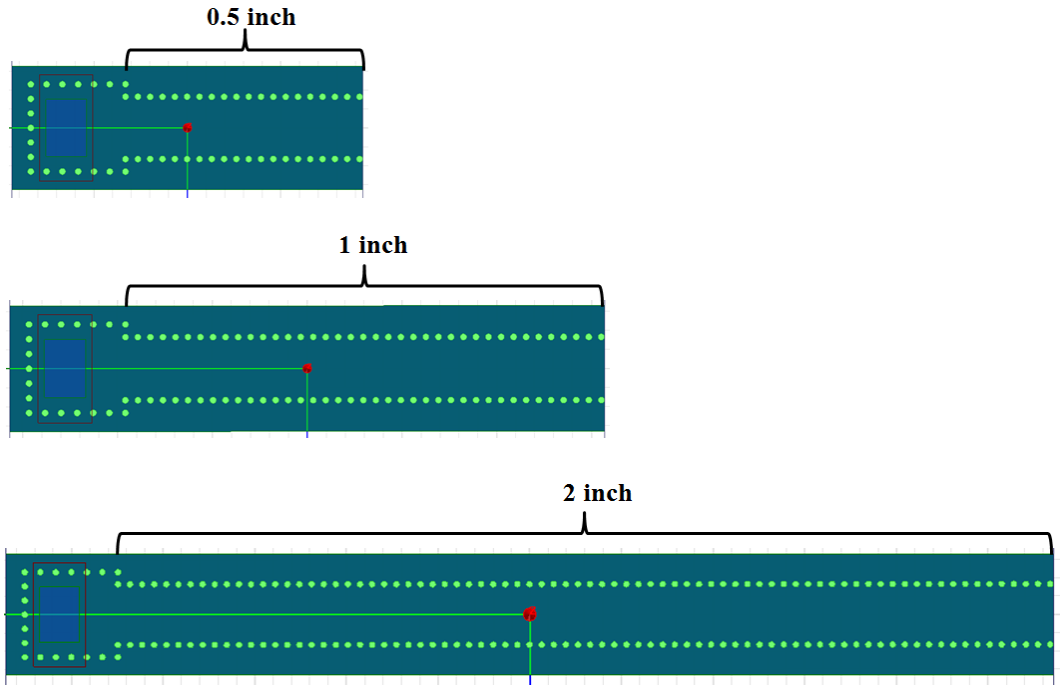

Figure 3.19 The simulation models (top view) of RWG-aperture transition-SIW structure with different-length core SIWs.

For the operative band 77-81 GHz, the simulation results for the whole structures with 0.5 inch long and 2 inch long core SIWs are shown in Figure 3.20 and Figure 3.21, respectively.

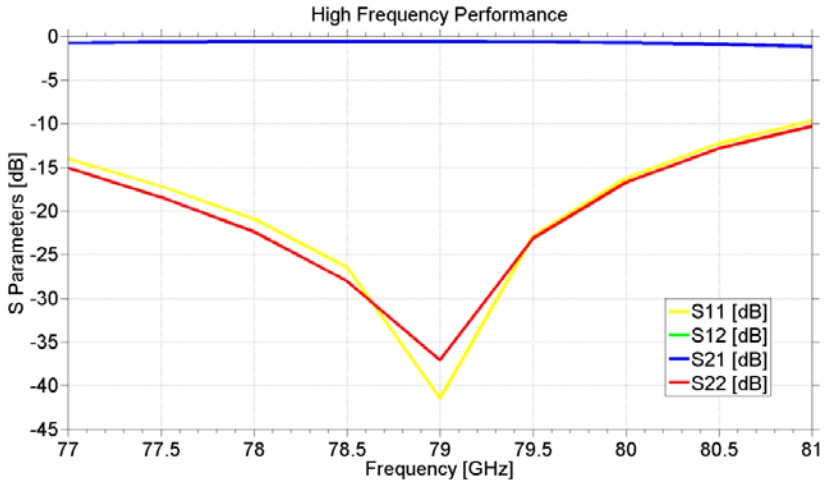

Figure 3.20 S parameters of the whole structure with 0.5 inch long core SIW for 77-81 GHz.

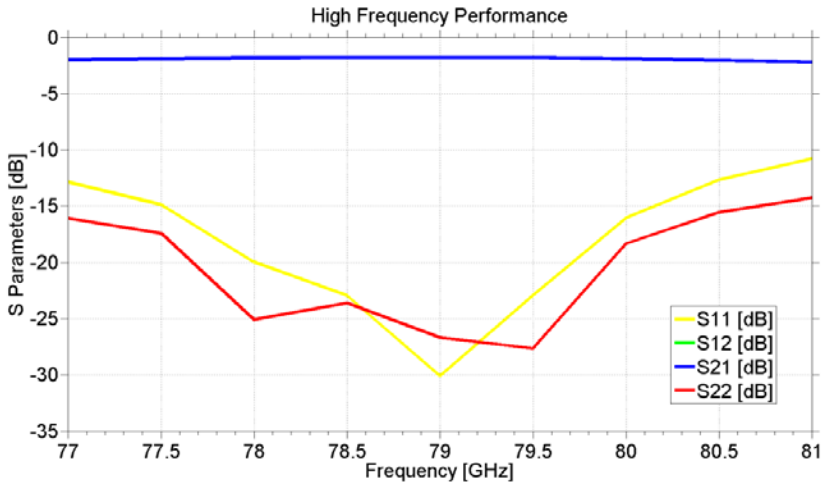

Figure 3.21 S parameters of the whole structure with 2 inch long core SIW for 77-81 GHz.

The simulated return loss S11 and insertion loss S21 for the whole structure with different-length core SIWs at specific frequencies (the central frequency and border frequencies) are shown in Table 3.5.

S11 / S21	0.5 inch	1 inch	2 inch
@ 77 GHz	-0.767 dB / -14.021 dB	-1.154 dB / -14.027 dB	-1.989 dB / -12.857 dB
@ 79 GHz	-0.606 dB / -41.474 dB	-1.008 dB / -27.640 dB	-1.781 dB / -30.069 dB
@ 81 GHz	-1.156 dB / -9.679 dB	-1.471 dB / -10.280 dB	-2.192 dB / -10.793 dB

Table 3.5 The return loss and insertion loss of RWG-transition-SIW structures for different-length core SIWs at 77 GHz, 79 GHz and 81 GHz.

From the data, make the best fitting lines and extract the insertion loss and return loss of the transition portion, which are shown in Figure 3.22 and Figure 3.23, respectively.

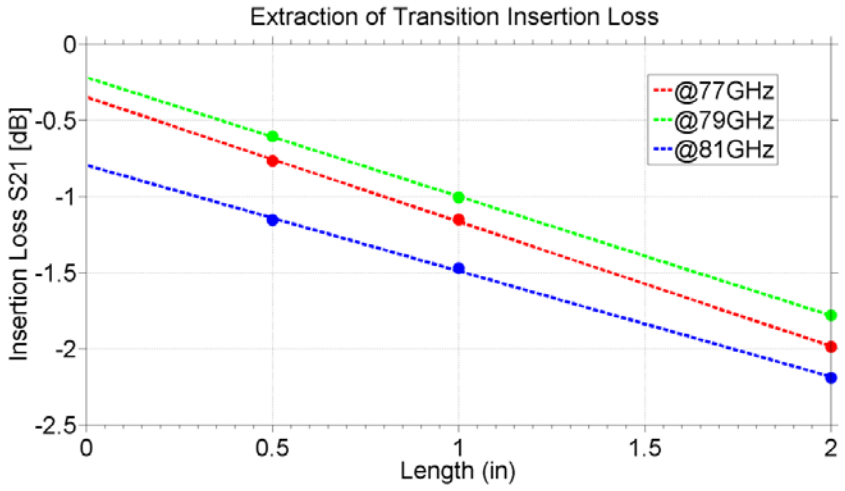

Figure 3.22 Insertion loss fitting and extraction for transition portion.

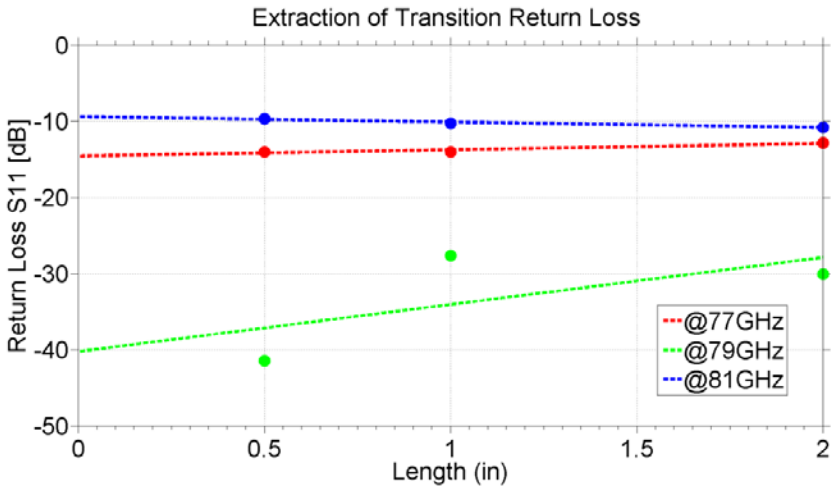

Figure 3.23 Return loss fitting and extraction for transition portion.

Calculate and get the loss of the transition portion (when Length = 0 inch) shown in Table 3.6 as below:

	@ 77 GHz	@ 79 GHz	@ 81 GHz
Insertion Loss	-0.3495 dB	-0.2195 dB	-0.7955 dB
Return Loss	-14.606 dB	-40.2595 dB	-9.4225 dB

Table 3.6 Aperture transition loss at specific frequencies.

For the operative band 56-68 GHz, the simulation results for the whole structures with 0.5 inch long and 2 inch long core SIWs are shown in Figure 3.24 and Figure 3.25, respectively.

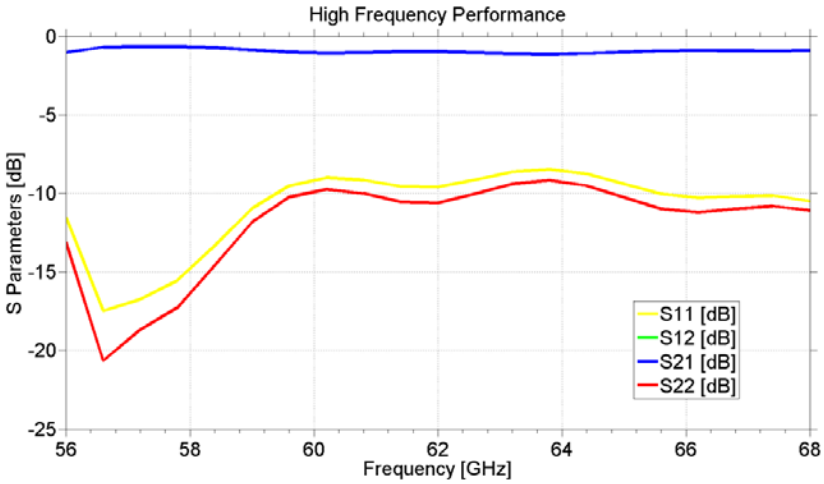

Figure 3.24 S parameters of the whole structure with 0.5 inch long core SIW.

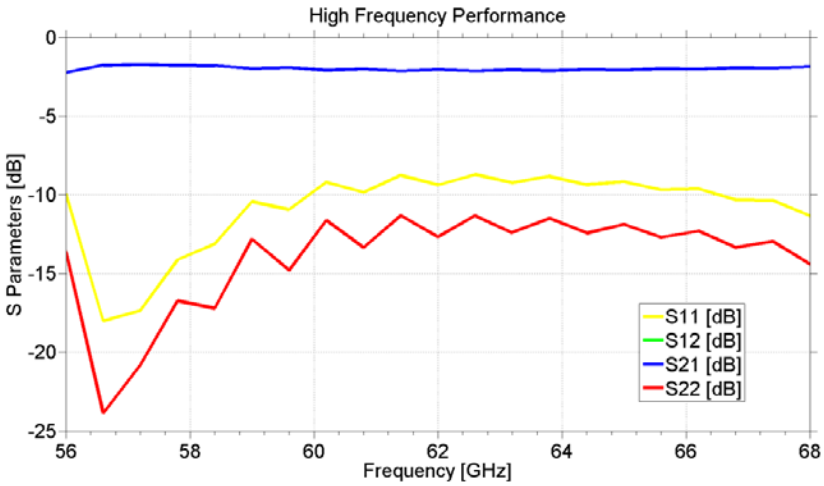

Figure 3.25 S parameters of the whole structure with 2 inch long core SIW.

For this operative band 56-68 GHz, the simulated return loss S11 and insertion loss S21 for the whole structure with different-length core SIWs at specific frequencies (the central frequency and border frequencies) are shown in Table 3.7.

S11 / S21	0.5 inch	1 inch	2 inch
@ 56 GHz	-1.021 dB -11.511 dB	-1.431 dB -10.837 dB	-2.244 dB -9.925 dB
@ 62 GHz	-0.978 dB -9.583 dB	-1.491 dB -8.476 dB	-2.051 dB -9.368 dB
@ 68 GHz	-0.898 dB -10.483 dB	-1.164 dB -11.396 dB	-1.855 dB -11.346 dB

Table 3.7 The return loss and insertion loss of RWG-aperture transition-SIW structures for different-length core SIWs at 56 GHz, 62 GHz and 68 GHz.

From the data shown above, make the best fitting lines and extract the insertion loss and return loss of the transition portion, which are shown in Figure 3.26 and Figure 3.27, respectively.

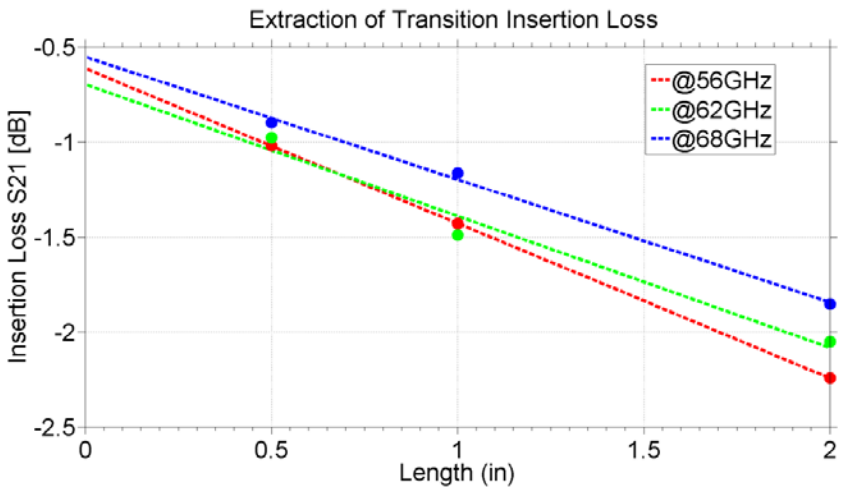

Figure 3.26 Insertion loss fitting and extraction for transition portion.

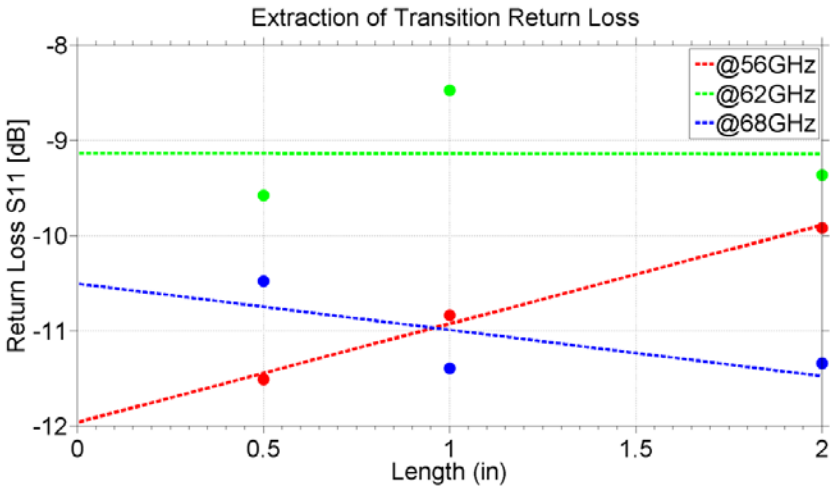

Figure 3.27 Return loss fitting and extraction for transition portion.

Calculate and get the loss of the transition portion (when Length = 0 inch) shown in Table 3.8 as below:

	@ 56 GHz	@ 62 GHz	@ 68 GHz
Insertion Loss	-0.6145 dB	-0.6980 dB	-0.5525 dB
Return Loss	-11.967 dB	-9.137 dB	-10.508 dB

Table 3.8 Aperture transition loss at specific frequencies.

For the operative band 40-50 GHz, the simulation results for the whole structures with 0.5 inch long and 2 inch long core SIWs are shown in Figure 3.28 and Figure 3.29, respectively.

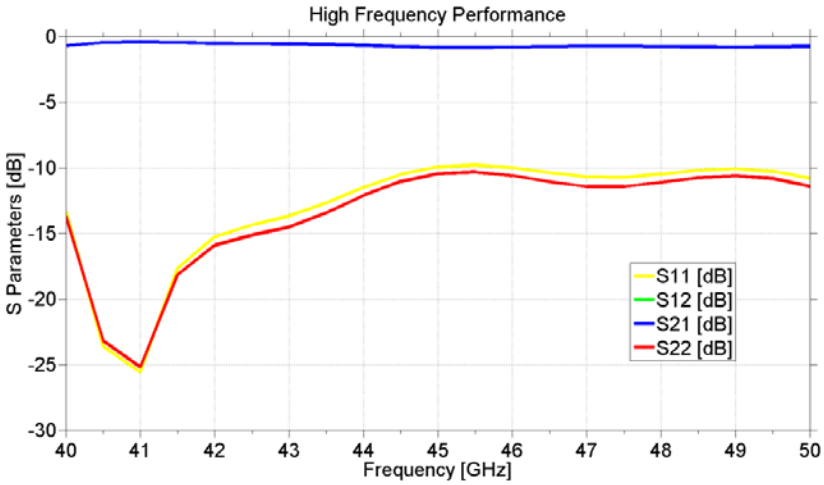

Figure 3.28 S parameters of the whole structure with 0.5 inch long core SIW.

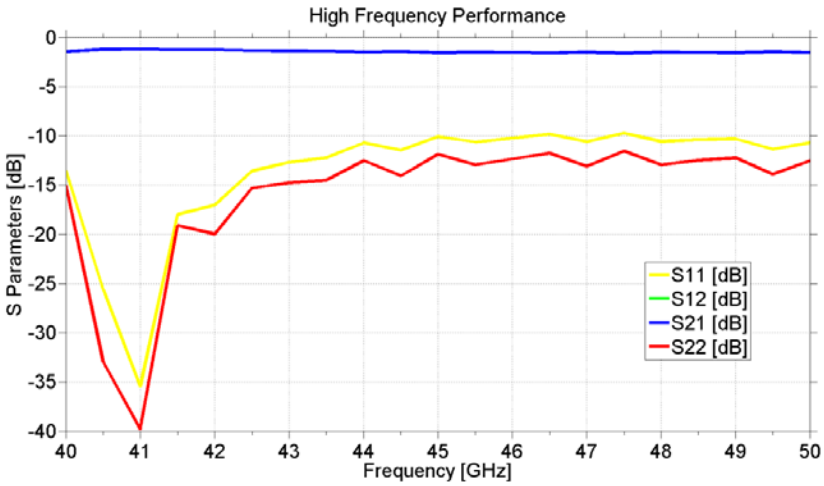

Figure 3.29 S parameters of the whole structure with 2 inch long core SIW.

For the band 40-50 GHz, the simulated return loss S11 and insertion loss S21 for the whole structure with different-length core SIWs at specific frequencies (the central frequency and border frequencies) are shown in Table 3.9.

S11 / S21	0.5 inch	1 inch	2 inch
@ 40 GHz	-0.693 dB / -13.334 dB	-0.844 dB / -15.466 dB	-1.437 dB / -13.550 dB
@ 45 GHz	-0.822 dB / -9.949 dB	-0.970 dB / -10.983 dB	-1.565 dB / -10.081 dB
@ 50 GHz	-0.745 dB / -10.823 dB	-0.966 dB / -11.230 dB	-1.529 dB / -10.696 dB

Table 3.9 The return loss and insertion loss of RWG-aperture transition-SIW structures for different-length core SIWs at 40 GHz, 45 GHz and 50 GHz.

Based on the data shown above, make the best fitting lines and extract the insertion loss and return loss of the transition portion, which are shown in Figure 3.30 and Figure 3.31, respectively.

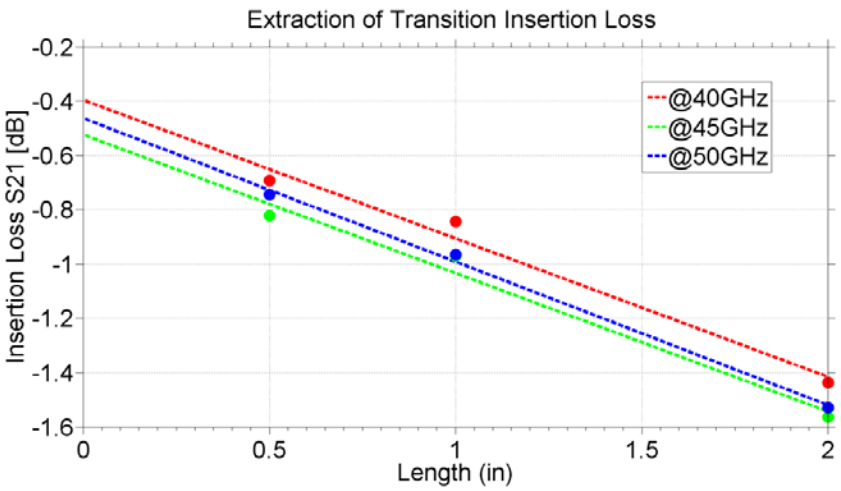

Figure 3.30 Insertion loss fitting and extraction for transition portion.

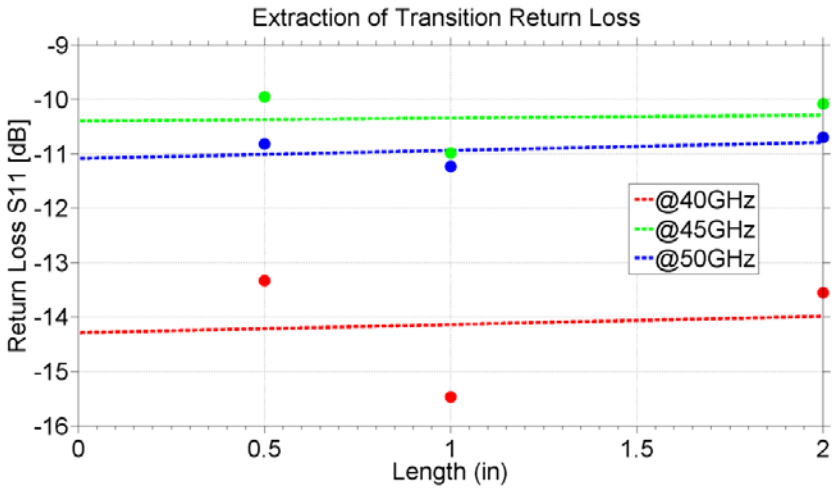

Figure 3.31 Return loss fitting and extraction for transition portion.

Calculate the insertion and return loss of the transition portion (when Length = 0 inch) and get the data shown in Table 3.10 as below:

	@ 40 GHz	@ 45 GHz	@ 50 GHz
Insertion Loss	-0.3965 dB	-0.5245 dB	-0.4635 dB
Return Loss	-14.292 dB	-10.4 dB	-11.09 dB

Table 3.10 Aperture transition loss at specific frequencies.

3.3 Optimization of Aperture Transitions with Genetic Algorithm

Since the high frequency performance of the aperture transitions described in chapter 3.2 are not good enough, especially for the 56-68 GHz and 40-50 GHz, then the dimensions and placements of the aperture transitions needs to be further optimized for these two operative bands. However, there are five dimensions (W,a, L, S and c shown in Figure 3.12) to be optimized, although they are physically separate, they react together and determine the input matching of transitions together. Thus, it is hard to find the optimal results or design by optimizing these dimensions or parameters one by one.

Genetic Algorithm (GA) is a directed random search technique to look for the optimal solution in complex multi-dimensional search spaces. Modelled on natural evolution, a GA uses genetic operators to manipulate individuals in a population over several generations to improve their fitness gradually, while each individual has a set of properties likened to chromosomes. Generally, there are three genetic operators: selection, crossover and mutation [23].

In this chapter, GA method is used to find the optimal dimensions and placements of the aperture transitions for the two operative bands--56-68 GHz and 40-50 GHz. Each individual has alterable five properties (chromosomes) – W (width of the aperture), a (width of the enlarged end of SIW), L (length of the aperture), S (center-to-center distance between the shorted circuit and aperture) and c (length of the enlarged end of SIW). Using the built-in Genetic Algorithm optimizer in HFSS, give the specific variable ranges for the values of these five chromosomes, set a population size of fifty to determine the mating pool, use the uniform crossover with a probability of 0.7, and implement the uniform mutation with a probability of 0.03. The GA runs until the design goal/fitness function is satisfied or 80 generations are reached. The fitness

function is defined as the return loss S11 values that exceed -12 dB at each discrete sampling frequency:

$$S11(f_i) \leq -12\ dB \qquad (3.2)$$

$$f_i = \begin{cases} 56, 57, 58, 59, 60, 61, 62, 63, 64, 65, 66, 67, 68 & for\ 56 - 68\ GHz \\ 40, 41, 42, 43, 44, 45, 46, 47, 48, 49, 50 & for\ 40 - 50\ GHz \end{cases} \qquad (3.3)$$

The new dimensions and displacements for the GA optimized aperture transitions are shown in Table 3.11 as below:

	W (mil)	L (mil)	S (mil)	c (mil)	a (mil)
56-68 GHz	58.5	73	51.5	238.5	128
40-50 GHz	92	148	74	210	221

Table 3.11 Optimized dimensions of the aperture transitions between RWG and SIW with GA.

The comparisons of high frequency performance between the original aperture transitions and the GA-optimized aperture transitions for 56-68 GHz are shown in Figure 3.32 (a) and (b), Figure 3.33 (a) and (b) and Figure 3.34 (a) and (b), respectively, while the whole RWG-transition-SIW structures with different-length (0.5 inch, 1 inch, and 2 inch) core SIWs are simulated, respectively.

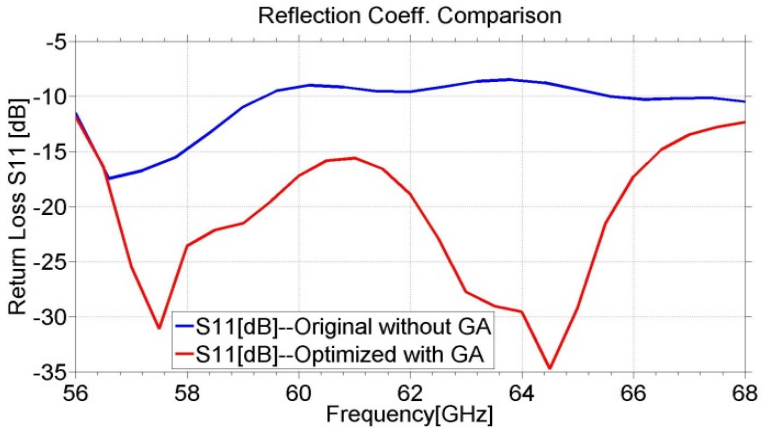

Figure 3.32 (a) Comparison of S11 between the original and optimized aperture transitions with 0.5 inch long core SIW for 56-68 GHz.

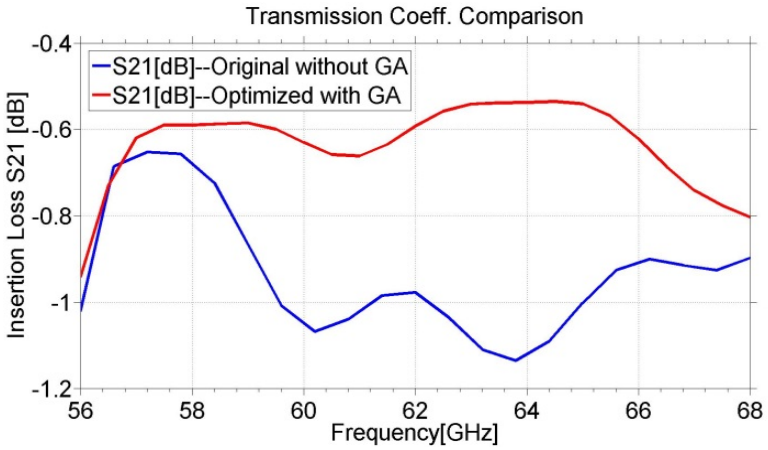

Figure 3.32 (b) Comparison of S21 between the original and optimized aperture transitions with 0.5 inch long core SIW for 56-68 GHz.

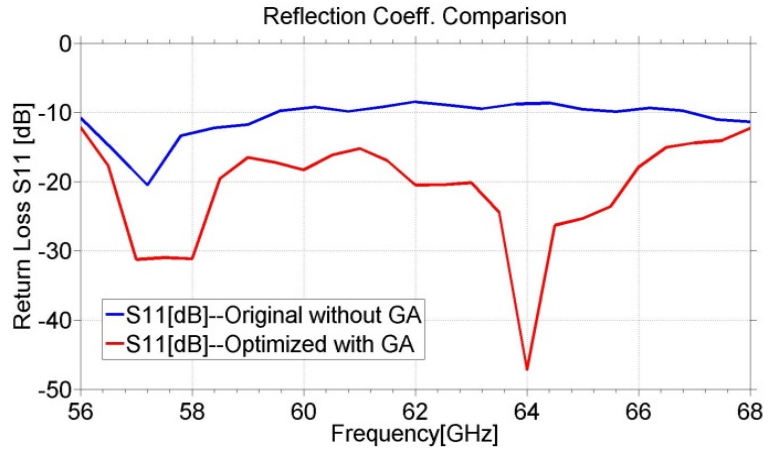

Figure 3.33 (a) Comparison of S11 between the original and optimized aperture transitions with 1 inch long core SIW for 56-68 GHz.

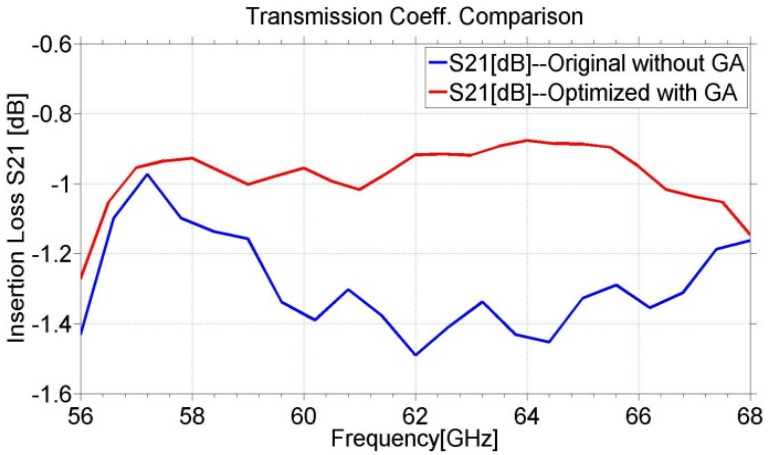

Figure 3.33 (b) Comparison of S21 between the original and optimized aperture transitions with 1 inch long core SIW for 56-68 GHz.

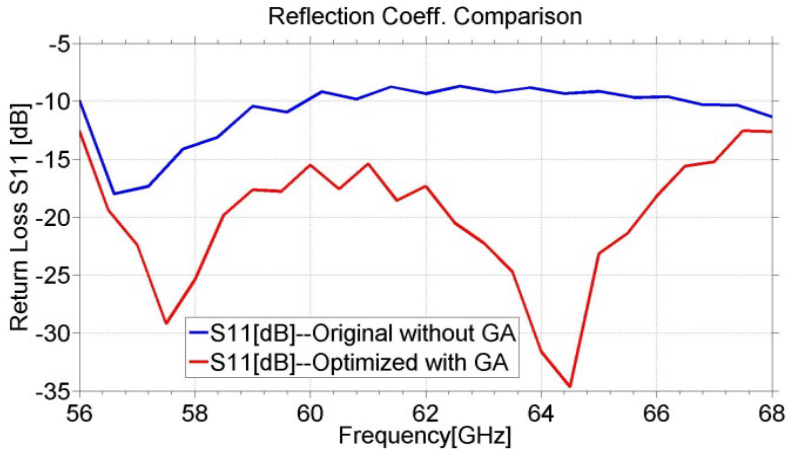

Figure 3.34 (a) Comparison of S11 between the original and optimized aperture transitions with 2 inch long core SIW for 56-68 GHz.

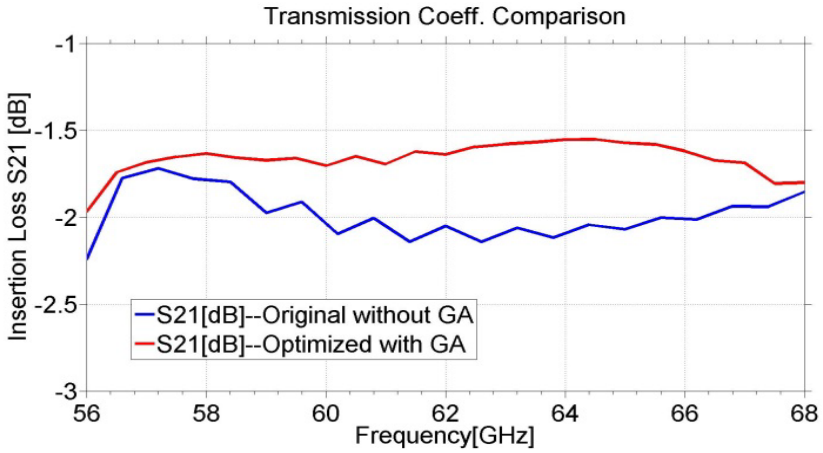

Figure 3.34 (b) Comparison of S21 between the original and optimized aperture transitions with 2 inch long core SIW for 56-68 GHz.

Also for 40-50 GHz, the comparisons of high frequency performance between the original and the GA-optimized aperture transitions are shown in Figure 3.35 (a) and (b), Figure 3.36 (a) and (b) and Figure 3.37 (a) and (b), respectively.

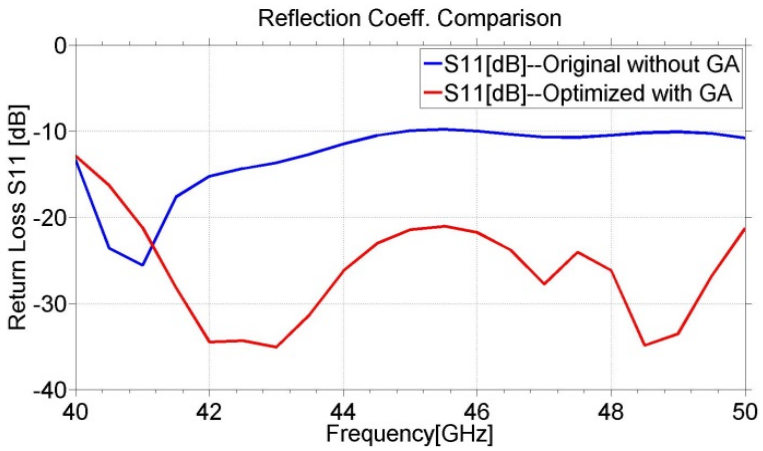

Figure 3.35 (a) Comparison of S11 between the original and optimized aperture transitions with 0.5 inch long core SIW for 40-50 GHz.

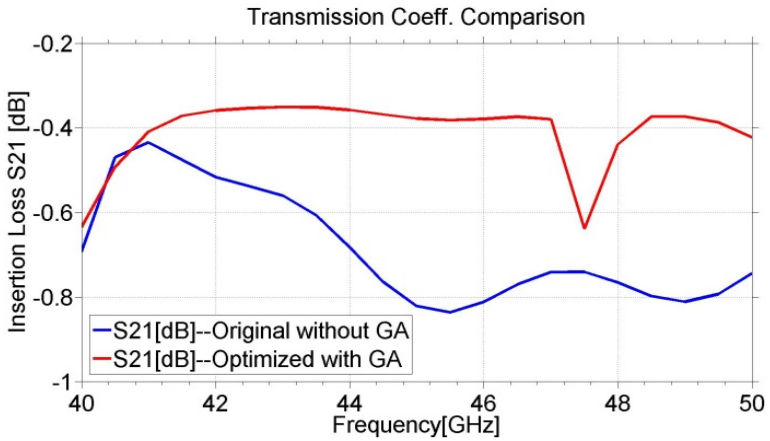

Figure 3.35 (b) Comparison of S21 between the original and optimized aperture transitions with 0.5 inch long core SIW for 40-50 GHz.

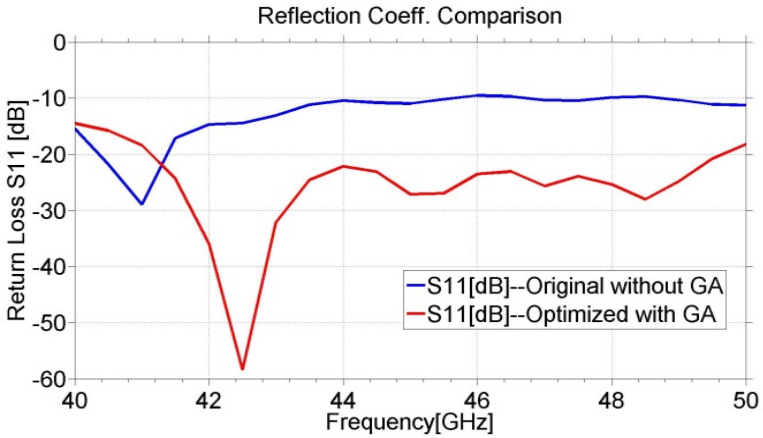

Figure 3.36 (a) Comparison of S11 between the original and optimized aperture transitions with 1 inch long core SIW for 40-50 GHz.

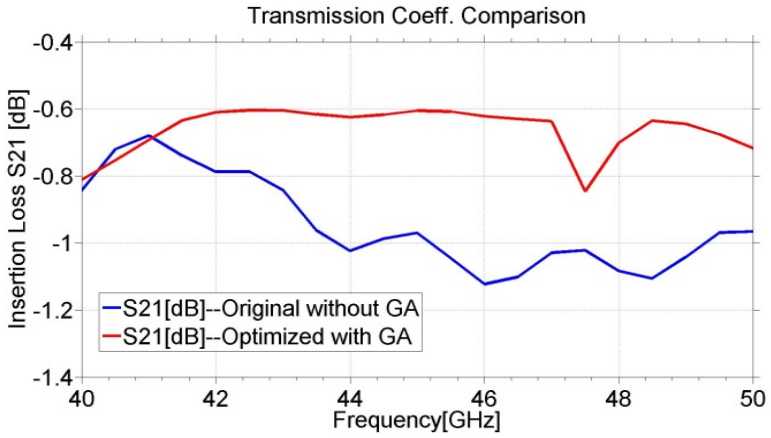

Figure 3.36 (b) Comparison of S21 between the original and optimized aperture transitions with 1 inch long core SIW for 40-50 GHz.

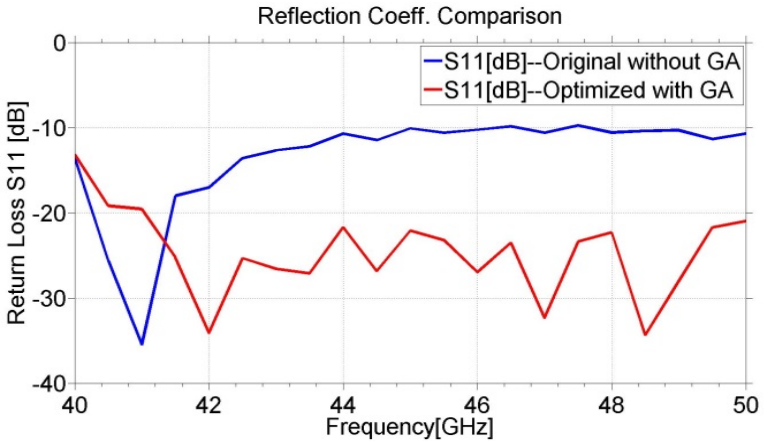

Figure 3.37 (a) Comparison of S11 between the original and optimized aperture transitions with 2 inch long core SIW for 40-50 GHz.

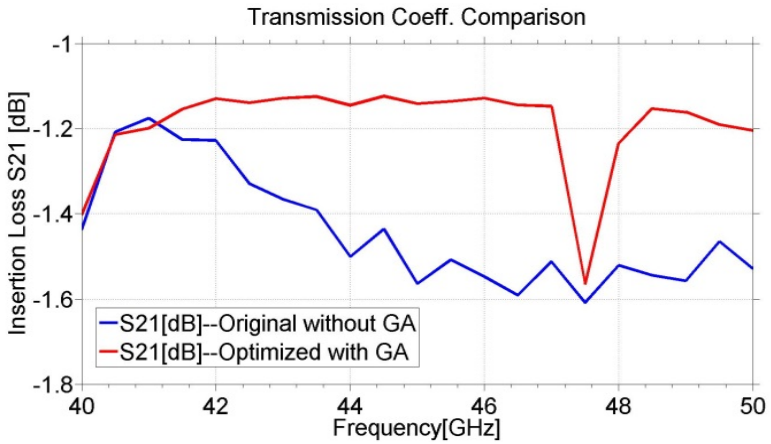

Figure 3.37 (b) Comparison of S21 between the original and optimized aperture transitions with 2 inch long core SIW for 40-50 GHz.

From the simulation results, we can see that though for a small number of frequencies, the performances of the optimized aperture transitions get worse, for the most part of operative bands, the performances get much better. Because the operative bands are very broad, it is hardly to guarantee the input matching is good for the whole working bands. The proposed GA optimization and its application to broadband transition design between RWG and SIW are feasible and effective.

Chapter 4

Conclusion and Future Work

In this work, we described the modeling method and design strategy of substrate integrated waveguide, and explored some parameters' influence on SIW high frequency performance, e.g. the center-to-center distance between both rows of vias affects the cutoff frequency of SIW. The loss minimization mechanics are studied and the loss minimization methods are proposed. E-band, V-band and Q-band substrate integrated waveguides are designed and simulated with HFSS, and their scattering parameters exhibit good high frequency performance. In order to show the advantages and disadvantages of SIW than other transmission lines, the RWG, stripline, microstrip line and GCPW counterparts of SIW are also designed and analyzed with HFSS. Although SIW has a little bit higher insertion loss than the other transmission lines, SIW has the great integration capability with other planar transmission lines which RWG lacks of, and SIW shows better compactness than RWG does; also SIWs almost do not have any mutual electromagnetic interference whey they are integrated in the same circuit, while the other transmission lines have mutual cross-talk phenomenon when they are integrated together.

We described the design strategy and optimization process for the RWG-to-SIW transitions. We etched a slot opening on the metallic layer of SIW to couple the energy between the RWG and SIW for narrow band (76-77 GHz), and etched a broader aperture on the metallic layer of SIW and broadened the width between vias around the aperture to couple energy for broad bands (77-81 GHz, 56-68 GHz and 40-50 GHz). A linear fitting method is used to extract the loss of the transition portion. The good high frequency performance of these transitions validate that the

design methods are feasible and reliable. The optimization of the broadband transitions using genetic algorithm provides a promising artificial intelligent method to search optimal solutions to optimization problems.

For the future work, we need to fabricate the real SIW and their transitions based on our design, do the measurements and analyze the measured data, to validate our simulation models. Also, we are studying other variants of SIW, such as HSIW (hollow substrate integrated waveguide) [24], to further decrease the dielectric loss or leakage loss of SIW. Furthermore, other forms of transitions between RWG and SIW needed to be explored to provide better energy transfer; meanwhile the transitions between SIW and other transmission lines such as GCPW and Microstrip are also deserve to explore. Moreover, since the genetic algorithm is not efficient enough to search the satisfied solution, or it will only find the local optimal solution but not the global optimal solution we actually need, we are studying other artificial intelligent methods to help us to optimize transition structures.

References

[1] H. Uchimura, T. Takenoshita and M. Fujii, “Development of a ‘Laminated Waveguide’ ,” *IEEE Transactions on Microwave Theory and Techniques*, vol. 46, no. 12, pp. 2438-2443, Dec. 1998.

[2] Y. Cassivi, L. Perregrini, P. Arcioni, M. Bressan, K. Wu and G. Conciauro, “Dispersion Characteristics of Substrate Integrated Rectangular Waveguide,” *IEEE Microwave and Wireless Components Letters*, vol. 12, no. 9, pp. 333-335, Sept. 2002.

[3] D. Deslandes and K. Wu, “Accurate Modeling, Wave Mechanisms, and Design Considerations of a Substrate Integrated Waveguide,” *IEEE Transactions on Microwave Theory and Techniques*, vol. 54, no. 6, pp. 2516-2526, Jun. 2006.

[4] F. Xu and K. Wu, “Guided-Wave and Leakage Characteristics of Substrate Integrated Waveguide,” *IEEE Transactions on Microwave Theory and Techniques*, vol. 53, no. 1, pp. 66-73, Jan. 2005.

[5] M. Bozzi, A. Georgiadis and K. Wu, “Review of Substrate-integrated Waveguide Circuits and Antennas,” *Microwaves, Antennas & Propagation, IET*, vol. 5, no. 8, pp. 909-920, Jun. 2011.

[6] D. Deslandes andKe Wu, “Integrated Microstrip and Rectangular Waveguide in Planar Form,” *IEEE Microwave and Wireless Components letters*, vol. 11, no. 2, pp. 68-70, Feb. 2001.

[7] D. Deslandes and Ke Wu, “Analysis and Design of Current Probe Transition From Grounded Coplanar to Substrate Integrated Rectangular Waveguides,” *IEEE Transactions on Microwave Theory and Techniques*, vol. 53, no. 8, pp. 2487-2494, 2005.

[8] D. Deslandes and Ke Wu, “Integrated Transition of Coplanar to Rectangular Waveguides,” *Microwave Symposium Digest, 2001 IEEE MTT-S International*, vol. 2, pp. 619-622, 2001.

[9] L. Xia, R. Xu, B. Yan, J. Li, Y. Guo and J. Wang, “Broadband Transition between Air-filled Waveguide and Substrate Integrated Waveguide,” *IET Electronics Letters*, vol. 42, no. 24, pp. 1403-1405, 2006.

[10] E. Moldovan, R. G. Bosisio and K. Wu, “W-Band Multiport Substrate-Integrated Waveguide Circuits,” *IEEE Transactions on Microwave Theory and Techniques*, vol. 54, no. 2, pp. 625-632, 2006.

[11] L. Li, X. P. Chen, K. Roni and K. Wu, “A Transition from Substrate Integrated Waveguide (SIW) to Rectangular Waveguide,” *Asia Pacific Microwave Conference 2009, IEEE*, pp. 2605-2608.

[12] R. Glogowski, J.-F. Zürcher, C. Peixeiro and J.R. Mosig, “Broadband Ka-band Rectangular Waveguide to Substrate Integrated Waveguide Transition,” *IET Electronics Letters*, vol. 49, no. 9, pp. 602-604, 2013.

[13] Q. F. Zhang and Y. L. Lu, “E-band ‘T’ Shape Transitions between Substrate Integrated Waveguide and Standard Waveguide,” *Asia Pacific Microwave Conference 2008, IEEE*, pp. 1-4.

[14] T. Kai, J. Hirokawa and M. Ando, “A Stepped Post-wall Waveguide with Aperture Interface to Standard Waveguide,” *IEEE Antennas and Propagation Society International Symposium*, vol. 2, pp. 1527-1530, 2004.

[15] M. Bozzi, L. Perregrini, K. Wu and P. Arcioni, “Current and Future Research Trends in Substrate Integrated Waveguide Technology,” *Radioengineering*, vol. 18, no. 2, pp. 201-209, 2009.

[16] H. Kumar, R. Jadhav and S. Ranade, “A Review on Substrate Integrated Waveguide and its Microstrip Interconnect,” *Journal of Electronics and Communication Engineering*, vol. 3, no. 5, pp. 36-40, 2012.

[17] R. Torres-Torres, G. Romo, B. Horine, A. Sanchez and H. Heck, “Full Characterization of Substrate Integrated Waveguides from S-Parameter Measurements,” *IEEE Electrical Performance of Electronic Packaging Conference*, pp. 277-280, 2006.

[18] E. Diaz, E. Miralles, H. Esteban, A. Belenguer, V. Boria, C. Bachiller, J. V. Morro and A. L. Borga, “Efficient and Accurate Design of Passive Devices in Substrate Integrated Waveguide Technology and their Tapered Transitions from Microstrip Lines,” *Waves* 3, pp. 76-85, 2011.

[19] http://www.microwaves101.com/encyclopedias/rectangular-waveguide-dimensions (Accessed on Mar. 18th 2015)

[20] I. Rosu, “Microstrip, Stripline, and CPW Design,” available at http://www.qsl.net/va3iul. (Accessed on Mar. 18th 2015)

[21] B. C. Wadell, “Microstrip Antenna Design Handbook,” Artech House, 1991, pp. 79.

[22] http://chemandy.com/calculators/coplanar-waveguide-with-ground-calculator.htm (Accessed on Mar.18th 2015)

[23] D. T. Pham, D. Karaboga, “Intelligent Optimisation Techniques. Genetic Algorithms, Tabu Search, Simulated Annealing and Neural Networks,” Springer, 2nd Edition, 2000.

[24] L. Jin, R.M.A. Lee, I. Robertson, “Analysis and Design of a Novel Low-Loss Hollow Substrate Integrated Waveguide,” *IEEE Transactions on Microwave Theory and Techniques*, vol. 62, no. 8, pp. 1616-1624, 2014.